HHS Public Access

Author manuscript

J Med Chem. Author manuscript; available in PMC 2020 February 14.

Published in final edited form as:

J Med Chem. 2019 February 14; 62(3): 1562–1576. doi:10.1021/acs.jmedchem.8b01754.

Discovery of Selective *Toxoplasma gondii* Dihydrofolate Reductase Inhibitors for the Treatment of Toxoplasmosis

Allen T. Hopper[a], **Adam Brockman**[a], **Andy Wise**[b], **Julie Gould**[b], **Jennifer Barks**[c], **Joshua B. Radke**[c], **L. David Sibley**[c], **Yongmao Zou**[d], and **Stephen Thomas**[a]

[a]Vyera Pharmaceuticals, LLC, 600 Third Avenue, 10th Floor, New York, NY 10016

[b]Evotec (UK) LTD, Alderley Park, Cheshire, UK SK104TG

[c]Department of Molecular Microbiology, Washington University School of Medicine, 660 S. Euclid Ave., St. Louis, MO 63130

[d]WuXi AppTec (Tianjin) Co., Ltd. 168 NanHai Road, 10th Avenue, TEDA, Tianjin (300457) P.R. China

Abstract

A safer treatment for toxoplasmosis would be achieved by improving the selectivity and potency of dihydrofolate reductase (DHFR) inhibitors, such as pyrimethamine (**1**), for *Toxoplasma gondii* DHFR (*Tg*DHFR) relative to human DHFR (*h*DHFR). We previously reported on the identification of meta-biphenyl analog **2**, designed by *in silico* modeling of key differences in the binding pocket between *Tg*DHFR and *h*DHFR. Compound **2** improves *Tg*DHFR selectivity 6.6-fold and potency 16-fold relative to **1**. Here, we report on the optimization and structure-activity relationships of this arylpiperazine series leading to the discovery of 5-(4-(3-(2-methoxypyrimidin-5-yl)phenyl)piperazin-1-yl)pyrimidine-2,4-diamine **3**. 2-Methoxypyrimidine **3** has a *Tg*DHFR IC_{50} of 1.57 ± 0.11 nM and a *h*DHFR to *Tg*DHFR selectivity ratio of 196, making it 89-fold more potent and 16-fold more selective than **1**. Compound **3** was highly effective in control of acute infection by highly virulent strains of *T. gondii* in the murine model and it

Corresponding Author Information: Allen Hopper, Sage Therapeutics, 215 First Street, Cambridge, MA 02142. Tel: 617-840-6026, allen.hopper@sagerx.com.

Present/Current Author Addresses: Allen Hopper (Sage Therapeutics, 215 First St., Cambridge, MA 02142; Adam Brockman (Cyprotex, 313 Pleasant St., Watertown, MA 02472; Andy Wise (Evotec (UK) LTD, Alderley Park, Cheshire, UK SK104TG; Julie Gould (Evotec (UK) LTD, Alderley Park, Cheshire, UK SK104TG; Jennifer Barks (Department of Molecular Microbiology, Washington University School of Medicine, 660 S. Euclid Ave., St. Louis, MO 63130; Joshua B. Radke (Department of Molecular Microbiology, Washington University School of Medicine, 660 S. Euclid Ave., St. Louis, MO 63130; L. David Sibley (Department of Molecular Microbiology, Washington University School of Medicine, 660 S. Euclid Ave., St. Louis, MO 63130; Yongmao Zou (WuXi AppTec (Tianjin) Co., Ltd. 168 NanHai Road, 10th Avenue, TEDA, Tianjin (300457) P.R. China; Stephen Thomas (Cerecor, 400 E. Pratt Street #606, Baltimore, MD 21202;

Author Contributions: ATH, AB and ST Lead optimization strategy; ATH, AB, AW, LDS and ST designed experimental strategies; AH, ST, YZ supported chemistry; AW, JB, JBR, JG conducted biological assays, ATH, AB, AW, JB, JBR, LDS, JG and ST analyzed data, ATH wrote the manuscript with input from all authors.

Supporting Information: Methods for *Tg*DHFR-TS protein purification and crystallization with **3** and **29** with diffraction and refinement statistics data. Methods for kinetic solubility, Log P, human and mouse liver microsome clearance, and MDCK-MDR1 permeability determinations. CEREP 44 cross-reactivity safety assessment data.

PDB ID Codes: Crystal structures of the TgDHFR-TS protein with bound compounds **3** and **29** have PDB ID codes **6n1t** and **6n1s**, respectively. Authors will release the atomic coordinates and experimental data upon article publication.

Disclosure Statement: AH, ST and AB are former employees of Vyera Pharmaceuticals.

possesses the best combination of selectivity, potency and prerequisite drug-like properties to advance into IND-enabling, pre-clinical development.

Graphical Abstract

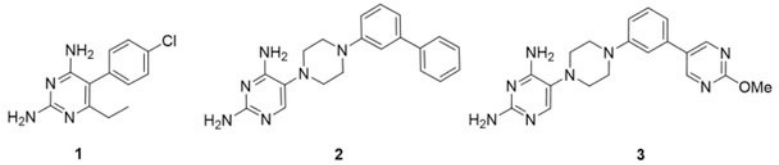

Compound	1	2	3
*Tg*DHFR[b] IC_{50} (nM)	140	8.8	1.6
hDHFR[c] IC_{50} (nM)	1,700	790	310
Selectivity (fold)[d]	12	79	200

[a]Pyrimethamine (**1**); [b]*T. gondii* DHFR; [c]human DHFR; [d]Selectivity: hDHFR/*Tg*DHFR

INTRODUCTION

Toxoplasmosis is caused by the protozoan parasite *Toxoplasma gondii* (*T. gondii*), an obligate intracellular parasite capable of infecting a wide range of hosts and many different types of cells[1]. Approximately one third of the population worldwide is chronically infected with various strains of *T. gondii*[2], with the seroprevalence being variable across the world. For example, *T. gondii* seroprevalence in the United States is estimated at about 10 to 15% of the population[3], it is >60% in Brazil, the Philippines, and Madagascar; 40% to 60% in Egypt, Argentina, and several European countries, including France, Germany and Poland; and 20% to 40% in Australia, Chile, Saudi Arabia and Iran[4–5]. Infections occur through consuming contaminated food or water, mother-to-child (congenital/vertical) and iatrogenic (transplanted organs and blood transfusion) transmission[6]. The parasitic infection is kept in check by the immune system where it exists in a latent bradyzoite form contained within tissue cysts that are commonly found in skeletal muscle and the central nervous system (CNS)[7]. However, in cases where the immune system is compromised, such as in a developing fetus or in patients with HIV, undergoing cancer chemotherapy or immunosuppressive treatment for organ transplantation, the parasite can transition to an active, fast replicating, and tissue damaging tachyzoite form[8]. Depending upon localization of the tachyzoites, active infection can cause, among other conditions, myocarditis, blindness and encephalitis; and is associated with a high mortality rate for HIV patients, even for those on active anti-retroviral treatment[8–11].

The recommended first-line treatment for toxoplasmosis is a combination therapy based on pyrimethamine (**1**) and sulfadiazine, supplemented with leucovorin (also known as folinic acid) to protect against bone marrow suyppression[11–12]. Pyrimethamine and sulfadiazine act synergistically on the folate metabolic pathway thereby inhibiting *T. gondii* proliferation and survival[13–14]. The drugs inhibit DHFR and dihydropteroate synthase (DHPS), respectively, and consequently block the synthesis of tetrahydrofolate, a key cofactor for thymidylate synthase. Thymidylate synthase is a methyl transferase that to produces deoxythymidine

monophosphate from deoxyuridine monophosphate. In many organisms including *T. gondii* and humans, this pathway is the only means by which thymidine can be supplied, making it essential for DNA synthesis and cellular proliferation[14–15]. Importantly, although the combination of pyrimethamine and sulfadiazine can control actively proliferating forms such as tachyzoites, these agents have little effect on the semi-dormant bradyzoite stages within tissue cysts and hence do not cure infection[16].

Adverse events associated with pyrimethamine-based therapy in toxoplasmosis often result in a need to reduce dosing or discontinue therapy[17]. The adverse events are mainly mechanism-based related to inhibition of folic acid metabolism in host tissues with high metabolic activity (e.g., epithelium and bone marrow)[18]. In mice, pyrimethamine has only about a 3-fold safety multiple between minimal effective dose and maximum tolerated dose[19]. Leucovorin, a form of tetrahydrofolate that is selectively taken up by human cells, is often co-administered to help alleviate the impact of mechanism-based toxicity to the host[20–23]. The use of pyrimethamine is also not suitable during the first trimester of pregnancy owing to its inhibition of human DHFR which can impact fetal organogenesis[23]. In addition, about 3% of the general population and 30% of patients with HIV/AIDS have a hypersensitivity reaction to the sulfonamide component of the treatment regimen[24–26]. Therefore, finding a standalone treatment would be of significant benefit to the HIV patient population most at risk of toxoplasmosis encephalitis and sulfa hypersensitivities. Finally, high doses of pyrimethamine can induce seizures, a likely consequence of off-target pharmacology[27]. The adverse events associated with pyrimethamine and sulfadiazine therapy could be reduced or eliminated by selectively inhibiting only the parasite DHFR. There have been numerous attempts to discover more selective inhibitors of *Tg*DHFR, but with limited success[28–32]. Recently, the crystal structure of *Tg*DHFR was solved[33]. This finding has enabled comparative modeling between the human and *T. gondii* enzymes, leading to the design and discovery of more selective *Tg*DHFR small molecules such as TRC-19 (**2**)[34].

Ideally, a next generation *Tg*DHFR inhibitor would have sufficient selectivity so that maximal parasiticidal activity would occur without concomitant inhibition of human *h*DHFR. Therefore, we hypothesized it would be important that the compound exhibit *Tg*DHFR to *h*DHFR selectivity of at least 150-fold, which is about 10-fold greater than that of pyrimethamine and possess low clearance to minimize maximal plasma concentrations while achieving a long duration of maximally effective exposure. Given the parasites ability to invade the CNS and cause significant harm upon reactivation of semi-dormant tissue cysts, it is also necessary that the compound readily penetrate the blood-brain barrier. Finally, improving *Tg*DHFR potency can reduce effective dose levels and decrease the likelihood of compound related off-target pharmacology and associated side effects and toxicity.

In this study, we report on the SAR and lead optimization strategy underlying the discovery of 5-(4-(3-(2-methoxypyrimidin-5-yl)phenyl)piperazin-1-yl)pyrimidine-2,4-diamine **3**, a selective and potent *Tg*DHFR inhibitor with properties consistent with those outlined above supporting a standalone treatment for toxoplasmosis.

RESULTS AND DISCUSSION

Pyrimethamine selectivity and potency.

Pyrimethamine **1** is reported to be 7.6-fold more selective for *Tg*DHFR compared to *h*DHFR with an IC_{50} of 760 ± 130 nM for inhibiting conversion of dihydrofolate to tetrahydrofolate[35]. In our hands, **1** has an IC_{50} for inhibiting *Tg*DHFR of 139 ± 49 nM (Figure 1), which makes it 12-fold more potent for inhibiting *Tg*DHFR over *h*DHFR. Although this level of selectivity is sufficient to make **1** a preferred DHFR inhibitor for the treatment of toxoplasmosis, as can be seen in Figure 1, it is not sufficient to preclude inhibition of hDHFR and associated dose limiting mechanism-based toxicity[36]. The concentration of **1** that gives significant inhibition of *Tg*DHFR, i.e., > IC_{80}, begins to also inhibit *h*DHFR by 5 to 35%. Based on these data, it seemed reasonable that at least an order of magnitude and preferably 20-fold increase in selectivity in a new compound would be sufficient to overcome the mechanism-based toxicity issues observed with **1** and possibly enable a standalone therapy.

Early profiling data for lead 2 and comparison to DHFR inhibitor reference standard drugs.

The structure of lead **2**[34] and DHFR inhibitor reference compounds pyrimethamine (**1**), trimethoprim (**4**), methotrexate (**5**) and trimetrexate (**6**) are shown in Figure 2. The DHFR inhibitory activity and selectivity, kinetic solubility, human liver microsomal intrinsic clearance and permeability and efflux across an MDR1-MDCK cell monolayer for lead **2** and reference compounds **1**, **4**, **5** and **6** are shown in Table 1. Lead **2** has a *Tg*DHFR IC_{50} of 8.76 ± 1.0 nM with 79-fold selectivity relative to the human enzyme. This is 6.6-fold more selective than **1**. Although this improvement in selectivity was encouraging, in our view is insufficient to achieve a stand-alone treatment. Trimethoprim **4**, sometimes used off label in combination with sulfamethoxazole for the treatment of toxoplasmosis, was about 240-fold less potent against *Tg*DHFR than **1** with an IC_{50} of 33,100 nM and selectivity index of 15. Methotrexate **5** was far more potent than **1**, **4** or **2** for inhibiting *h*DHFR with an IC_{50} of 4.74 nM. Interestingly, **5** has the opposite selectivity profile as compared to **1**, where it is 17-fold less potent for inhibiting *Tg*DHFR (IC_{50} of 78.3 nM), giving a selectivity ratio of 0.061. Trimetrexate **6**, which structurally is a combination of the diaminopteridine head of **5** and trimethoxybenzyl tail of **4**, is nearly equally active at *Tg*DHFR and *h*DHFR with respective IC_{50}'s of 1.35 and 4.07 nM, giving a selectivity index of 3.0.

Further characterization of **1** and **2** was performed to benchmark and guide a lead optimization strategy (Table 1). Lead **2** has low kinetic and thermodynamic solubility (< 4 μM), high clearance in human liver microsomes (HLM) (i.e. > liver blood flow), and low to moderate MDCK-MDR1 permeability, all areas for improvement during lead optimization. Interestingly, **1**, which was discovered and developed in the 1940s, has near ideal CNS drug properties in terms of solubility, HLM stability and MDR1-MDCK permeability. Properties for **1** and **2** are summarized in Table 2, with the main differences being an increase in both MW and log P for **2**, which likely contributes to its undesirable solubility, metabolic stability and permeability profile. Based on these data, lead optimization was initially focused on understanding the SAR underlying selectivity and potency, while simultaneously designing

analogs with lower cLog P and higher calculated solubility in an effort to improve physical chemical properties.

Structure-activity relationships for analogs of 2.

Structure activity relationship (SAR) data based on **2** for inhibition of *Tg*DHFR and selectivity relative to *h*DHFR are shown in Tables 3–5. Initial optimization of **2** focused on a systematic approach to gain a better understanding of its SAR with emphasis on improving DHFR selectivity (Table 3). As a basis for comparison, unsubstituted analog **7** was prepared and found to lose potency (IC_{50} 209 nM) but maintained a similar selectivity index (59-fold) relative to initial lead **2**. Ortho-phenyl **8** and para-phenyl **9** were both about 4-fold less potent (IC_{50} ~ 30 nM) than **2** but differed in their selectivity profiles. Ortho-phenyl **8** maintained similar selectivity as **2** at 58-fold, whereas para-phenyl **9** had reduced selectivity at 11-fold. These data are consistent with modeling predictions of the binding cavity[34]. Replacing the distal meta-phenyl of **2** with an ortho-methyl **10** or ortho-chloro **13** resulted in complete loss of activity at the highest doses tested. This result is surprising considering ortho-phenyl analog **8** had a *Tg*DHFR IC_{50} of 31 nM. Meta-methyl and meta-chloro analogs **11** and **14**, respectively, were more potent and selective than corresponding para-substituted compounds **12** and **15**, supporting the hypothesis based on modeling that meta-substituents would be preferred. Encouragingly, meta-methyl **11** while 8-fold less potent than **2**, maintained equivalent selectivity of 79-fold. Based on these findings, design focused on meta-substituents to further probe this apparently important pocket for both selectivity and potency. Meta-methoxy **16**, meta-trifluoromethyl **17**, meta-trifluoromethoxy **18** and meta-cyclopropyl **19** all had reduced potency and selectivity as compared to meta-phenyl lead **2**. Adding a methyl or ethyl to the 6-position of the diaminopyrimidine group, giving **20** and **21** respectively, maintained or slightly improved potency over **2**, but with a slight loss in selectivity.

Structure-activity relationships for heteroaryl analogs of meta-biphenyl 2.

We then turned our focus toward improving the solubility and metabolic stability issues observed with early lead **2** by preparing a variety of heteroaryl analogs (Table 4). We hypothesized that the distal phenyl ring of **2** was the likely site of metabolism and that introducing nitrogen molecules into this ring would block metabolism and increase solubility. The 2-, 3- and 4-pyridine analogs **22**, **23** and **24** maintained or slightly improved potency and selectivity, but without much improvement in solubility. The potency of 3-pyridine analog **23** is noteworthy at 2.7 nM, about 3.3-fold more potent than **2**, and with a selectivity index of 112-fold. Addition of a second nitrogen into this ring to give pyrimidines, pyridazines and pyrazines provided analogs with variable improvements in potency, selectivity, solubility and HLM metabolic stability. 5-Pyrimidine analog **26** stood out with a 307-fold *Tg*DHFR selectivity index and a *Tg*DHFR IC_{50} of 5.2 nM, as well as markedly improved solubility (>200 uM) and metabolic stability (Clint < 8.6 mL/min/kg). The improvement in selectivity observed for **26** is nearly 4-times that of early lead **2** and 25-fold better than **1**. 2-Pyrazine **27** and 4-pyridazine **28** had promising potency with IC_{50}s of 10 and 6.0 nM respectively, and selectivity indexes of 129 and 185-fold respectively, but both were hampered with low kinetic solubility, precluding additional investigation with

these chemotypes. In general, heteroaryl substitutions increase *Tg*DHFR selectivity and maintain or slightly improve potency relative to **2**. The two-fold improvement in selectivity observed for 5-pyrimidine analog **26** compared to the 3-pyridyl analog **23** may result from one of the nitrogen atoms on the distal pyrimidine ring being forced to make an unfavorable interaction in hDHFR. The 3-pyridyl analog **23**, which can rotate the nitrogen away from such an unfavorable interaction is about 5-fold more potent at hDHFR than pyrimidine **26 (**hDHFR IC_{50} 1430 nM**)**.

SAR for the distal 5-pyrimidine ring of 26.

Next, we evaluated if selectivity could be further improved by adding substitutions onto the 2-position of the distal 5-pyrimidine ring of **26** (Table 5). Based on the crystal structure and modeling (see Figures 3 and 4), it appeared that substitutions at this position were not likely to have steric effects as they pointed into solvent space. However, if the pyrimidine nitrogen atoms were making a favorable hydrogen bond interaction with *Tg*DHFR His-27 and an unfavorable interaction with hDHFR Pro-26, then electron donating substituents would be predicted to enhance potency and selectivity. Methyl analog **29** maintained *Tg*DHFR potency (IC_{50} 3.95 nM) with only a slight reduction in selectivity (237-fold) relative to unsubstituted 5-pyrimidine **26**. Methyl analog **29** had good solubility, HLM stability and MDCK-MDR1 permeability. An electron donating 2-methoxy substituent gave **3**, with excellent *Tg*DHFR potency with an IC_{50} of 1.57 nM, but a slightly reduced selectivity index of 196. Trifluoromethyl **30** and cyclopropyl **31** were significantly less potent against *Tg*DHFR, less selective and had low kinetic solubility. The loss in selectivity with these analogs is principally driven more by loss of activity against *Tg*DHFR rather than by gaining potency at hDHFR.

Further characterization of **3** demonstrated good kinetic solubility of 186 μM at pH 7.4, low human microsomal clearance (<8.6 mL/min/kg) and high permeability in MDR1-MDCK cells (20.1×10^{-6} cm/s) with a low efflux ratio of 1.1 (Table 5). In the CEREP 44 safety screen at a 10 μM dose level, **3** demonstrated good selectivity against all 44 targets tested, except for hERG where [^{3}H] Dofetilide binding was inhibited by 60%.

Chemistry.

The compounds presented here were synthesized as shown in Schemes 1 and 2. In Scheme 1, substituted piperazines (**36a-n**) were condensed with 5-bromouracil **33** in the presence of KF and heating in DMSO to give the corresponding uracil derivatives **37a-n**. Chlorination using $POCl_3$ and DIPEA provided intermediates **38a-n**, followed by amination reaction using NH_3/EtOH at 145 °C to give final products **2, 7–18, 20, 21 and 32**. 6-Methyl and 6-ethyl diaminopyrimidine targets **20** and **21** were synthesized as described above, but starting with the corresponding 6-alkyl-5-bromouracils **34** and **35** and condensing with biphenyl-piperazine **36a.** Piperazine intermediates **36a-n** are generally commercially available or can be prepared by various literature methods[37–38].

Analogs in Scheme 2 were prepared by either Suzuki coupling of 3-bromophenyl **32** with the corresponding boronic acids **39o-w** to give targets **3, 19, 23, 24, 26** and **28–31**, or Stille coupling of 3-bromophenyl **32** with $Sn(Bu)_3R^2$ **40x-z** to generate compounds **22, 25** and **27**.

Crystal structure of *Tg*DHFR.

To aide in the understanding of the observed selectivity and guide future lead optimization efforts, several X-ray crystal structures with lead compounds bound to *Tg*DHFR were solved, including the complex of 5-pyrimidines **3** and **29** with *Tg*DHFR (Figures 3 and 4). Although at a high-level these data are consistent with modeling predictions, the crystal structure provides more subtle clues into why the distal pyrimidine moiety enhances selectivity. The phenyl groups of **3** and **29** occupy the *Tg*DHFR cavity created near F91 and G22 (Figure 4), while the residues present in *h*DHFR at these positions appear to be less accommodating. These *Tg*DHFR phenylalanine residues (F32 and F91) create a more enclosed hydrophobic area around the phenyl ring connected to the piperazine. This configuration also positions the distal heteroaromatic ring into the glycine site, possibly enabling a hydrogen bonding interaction with His 27 in the *T. gondii* enzyme (Figure 3). The presence of a proline residue (Pro26) in *h*DHFR, at the analogous position of His 27 in *Tg*DHFR, provides a hypothesis for the observed subtle improvement in selectivity with the 5-pyrimidines. The *Tg*DHFR His27 may enable a favorable H-bond with a pyrimidine N, whereas this would not be feasible in the human enzyme. In addition, there could be an unfavorable interaction in the *h*DHFR between the pyrimidine nitrogen atoms of **3** and Pro 26. This interaction might help explain why 3-pyridine **23** is less selective than pyrimidine **3**, as the pyridine N could rotate away from the proposed unfavorable interaction with Pro26 in the human enzyme. We hypothesize these are the likely reasons for the observed *Tg*DHFR selectivity. However, it is also noted that, N64 in *h*DHFR blocks π-π interactions. Interactions at these residues are well supported by the literature and may also contribute to the observed *Tg*DHFR selectivity[39]. A search of UniProt shows that there are no reported human polymorphisms related to these amino acids that would alter selectivity[40].

Parasiticidal and anti-proliferative effects of 5-methoxypyrimidine 3 in cell-based models.

Optimized pyrimidine **3** and comparator drug **1** were evaluated in cell-based models to investigate translation of the respective DHFR inhibitory activities into parasiticidal and antiproliferative host cell effects. Lead **3** had a parasiticidal EC_{50} of 13 nM and **1** had an EC_{50} of 680 nM against the type I RH strain of *T. gondii*. The 52-fold improvement in potency of **3** over **1** in this assay is consistent with its 89-fold potency advantage for inhibiting *Tg*DHFR. Antiproliferative effects of these compounds in human MCF-7 cells, measured using the MTT assay, were consistent with the human DHFR data, wherein **1** and **3** had EC_{50}s of 11,600 nM and 7,300 nM, respectively. The selectivity of both **1** (17-fold) and **3** (560-fold) in the cell-based assays (Table 6) is in line with their DHFR selectivity profiles of 12 and 200-fold, respectively. These data are important as they demonstrate that **3** has anti-parasiticidal activity with similar efficacy as **1**, but with substantially better potency and selectivity.

Comparison of potency against additional strains of Toxoplasma.

Given the enhanced potency of **3**, we wanted to test it against different lineages of *T. gondii*. Consequently, we chose a series of low passage isolates that are representative of the major genotypes of *T. gondii* seen in human infection from different regions of the world. As we have previously described, the population structure of *T. gondii* is comprised of 6 major

clades, each of which contains several related lineages[41]. The majority of human cases of toxoplasmosis in Europe and North America are due to type 2 strains[42–44], and we typically use a laboratory strain called ME49 as representative for such strains. The ME49 strain was originally isolated from a sheep in the United States[45], and it reflects the genotype of many strains found in food animals and which cause human toxoplasmosis. Type 1 strains are also reasonably abundant in North America, and they are of interest as they are more pathogenic in many hosts including immunocompromised humans[44, 46] Although most lab studies use the type 1 RH strain, use of the GT1 strain is preferable as it preserves the entire lifecycle[47]. The GT1 strain was originally isolated from a goat in North America[48], although it is genetically similar to a number of human isolates including the RH strain. In contrast to North America and Europe, strains in South America are dominated by highly pathogenic lines such as types 5 (reference strain RUB) and 10 (reference strain VAND)[41]. The VAND and RUB strains were isolated from severe human cases of toxoplasmosis that are characteristic of the Amazon region[49–50]. These strains have also been used as reference strains for the Toxoplasma comparative genomes paper[51].

To monitor the effects of new antiparasitic compounds on different strains of *T. gondii* we generated fire fly luciferase (FLUC) expressing lines so that we could use a common luciferase-based growth assay to monitor growth inhibition. We compared the potency of **3** for its ability to inhibit the growth of *T. gondii* strains in vitro. As shown in Table 7, the potency of **3** was highly similar across these different lineages, with only 2 to 3-fold differences being observed in potency. The FLUC lines used here also carry a pyrimethamine resistance allele of DHFR that was used to generate the transgenic lines. This resistant DHFR allele confers highly level resistance to pyrimethamine as described previously[52], but interestingly this does not lead to cross-resistance to **3**.

Mouse pharmacokinetic and brain to plasma exposure studies.

2-Methoxypyrimidine **3** was selected over 2-methylpyrimidine **29** and unsubstituted pyrimidine **26** for further in vivo characterization owing to its substantially improved stability in mouse liver microsomes (MLM). Preclinical models of toxoplasmosis are primarily performed in mice and therefore a compound with sufficient oral bioavailability, and plasma and CNS exposure to support murine efficacy testing was desired. Fortunately, **3** had moderate mouse liver microsome (MLM) intrinsic clearance (Clint) of 56.3 mL/min/Kg, which is 63% of mouse liver blood flow (LBF), whereas **29** and **26** both had high predicted clearance with MLM Clint values of 431 and 2,700 mL/min/Kg, respectively, multiples above mouse LBF. The oral and IV PK parameters in mouse are summarized in Table 8. Compound **3** has low to moderate clearance of 10.6 mL/min/kg, a volume of distribution of 1.14 L/kg and a half-life of 3.9 h after a 1.0 mg/kg, iv dose. Oral bioavailability after a 0.83 mg/kg, po dose was 47.3% with a Cmax of 178 ng/mL 30 minutes after dosing. The unbound fraction (%) in mouse plasma is 8.7 ± 0.2 and in brain homogenate 2.4 ± 0.3, determined using an equilibrium dialysis method. Compound **3** was freely permeable into the mouse CNS at 0.5 hours after a 10 mg/kg oral dose, the concentration in brain was 2,560 ± 240 ng/g and in blood 1,610 ± 580 ng/mL giving a brain to blood ratio of 1.7 ± 0.6.

In vivo efficacy of 1 and 3 in a murine model of acute Toxoplasmosis.

Compounds **1** and **3** were tested independently in a murine model of acute toxoplasmosis and observed to improve survival in a dose-dependent manner (Figures 6a and 6b). Female CD-1 mice were inoculated intraperitoneally (IP) with 3,000 tachyzoites of the highly virulent RH strain of *T. gondii* on Day 0. In parallel, 3 negative control mice were inoculated with vehicle, lacking the parasite. The parasite strain used in this study was genetically modified to constitutively express the enzyme luciferase and enable infection monitoring via an in vivo imaging system (IVIS®)[53]. Mice were monitored for survival for 30 days with intermittent IVIS monitoring (data not shown). On day 4 of dosing, compound exposure was assessed by micro-sampling from tail vein from 3 mice per group at 1, 4 and 12 h post-dose and 3 mice per group at 2, 8 and 24 h post-dose (data shown in Figures 7a and 7b).

Compound **3** at doses of 10 mg/kg, QD or BID for 7 days, yielded 100% survival for 30 days (end of study), while doses of 1 and 3 mg/kg produced similar results on survival as comparator compound **1** did at 18 mg/kg BID and 54 mg/kg QD, respectively. Survival data for **1** in this study were consistent with published literature[54–56]. All mice treated with vehicle died within 6 to 7 days. It should be noted that the single animals that were lost in the 3 mg/kg compound **3** group and 54 mg/kg compound **1** group were believed to be due to handling errors during imaging rather than active *T. gondii* infection as no signs of infection or bioluminescence (data not shown) were observed for these animals during the study. Consistent with the improved in vitro potency of **3** relative to **1**, it was also more potent in vivo producing similar efficacy at doses about 18-fold lower.

Cure rates were assessed by subinfection of naive mice with combined homogenized brain and lung tissue from mice that survived 30 days. The tissues from two surviving mice of the same dosing group were injected into one donor mouse. Infection with a single *T. gondii* parasite of the type I RH strain is believed to be 100% lethal in naive mice[47]; therefore, sub-inoculated naive mice that survived for 15 days and were without signs of infection, was indicative of a cure (i.e., the donor mice were devoid of parasite). It should be noted that the RH strain of *T. gondii* does not typically form tissue cysts. Therefore, a cure in this model may not translate to a cure with clinically relevant strains that form tissue cysts. Nonetheless, it is clear both **1** and **3** are strongly efficacious in eradicating the tissue damaging and life threating tachyzoite form of the parasite.

Compound **3** had a cure rate of 50% in the 1 and 3 mg/kg groups and 100% in the 10 mg/kg groups. Pyrimethamine **1** was 100% curative at the 54 mg/kg dose and 33% to 67% curative at the 18 mg/kg BID dose. These data suggest that inhibition of *Tg*DHFR is sufficient for maximal efficacy as a stand-alone therapy (e.g., without coadministration of a DHPS inhibitor). Regarding the results for pyrimethamine **1**, the human equivalent dose of 54 mg/kg in mouse (approximately 300 mg/day in a 70-kg individual) cannot be administered in patients owing to dose-limiting, mechanism-based safety issues.

For both compounds, the onset of effect on survival time occurred at exposures near or slightly above the *T. gondii* cell-based EC_{50} values (1.0 mg/kg for **3** and 18 mg/kg for **1**), with maximal effects occurring at dose levels of 3 mg/kg and 10 mg/kg for **3** and 54 mg/kg for **1** (Figures 7a and 7b), which exceed the cell-based EC_{50}s.

CONCLUSIONS

Rational drug design led to the identification of several highly selective and potent arylpiperazine-based *Tg*DHFR inhibitors. The structure-activity relationship for these compounds provides proof-of-concept for the feasibility of discovering a next generation toxoplasmosis treatment with improved potency, selectivity, and safety. 2-Methoxypyrimidine **3**, with 16-fold better selectivity for *Tg*DHFR and 89-fold better potency as compared to pyrimethamine **1**, and desirable DMPK and safety properties, was selected for exploration in preclinical models of toxoplasmosis. Compound **3** was effective in radical cure of acute infection with the highly virulent type I RH strain in the murine model and showed similar potency across multiple parasite lineages in cell-based parasite growth assays. Based on the efficacy observed, we hypothesize it will be feasible to achieve parasiticidal levels of **3** in patients that are below concentrations that would inhibit *h*DHFR, thus providing a safer and more efficacious therapy than is currently available and possibly obviating the need for sulfonamide combination therapy.

EXPERIMENTAL SECTION

Materials and Methods.

General.—All synthetic chemistry, DMPK, *T. gondii* DHFR crystal structures with **3** and **29**, and DHFR in vitro pharmacology was performed at WuXi App Tec at their China facilities in Tianjin and Shanghai. Work with *Toxoplasma gondii* was performed at Evotec in Manchester, UK and in Prof. Sibley's lab at Washington University, St. Louis. Proton NMR spectra were recorded on a Varian 400 MHz NMR. LCMS were taken on a quadrupole Mass Spectrometer on Shimadzu LCMS 2010 (Column: sepax ODS 50×2.0 mm, 5 μm) or Agilent 1200 HPLC, 1956 MSD (Column: Shim-pack XR-ODS 30×3.0 mm, 2.2 μm) operating in ES (+) ionization mode. All final compounds were greater than 95% pure based on HPLC UV% AUC. Structures were determined by ^{1}H NMR and LC/MS. Final compounds in this manuscript are not known to interfere with the assays here in (i.e., they are not PAINS).

All animal studies were conducted at WuXi App Tec in China and Evotec in Manchester, UK and were performed in accordance with the institutional guidelines for these Countries and Laboratories.

LC/MS Methods

Method A: Run on a Shimadzu LC-20AB with a MS 2010 detector using a Luna-C18(1) column (2.0*30mm, 3um) at 40 °C. Mobile phase A was 0.037% (v/v) aqueous TFA and mobile phase B was 0.018% (v/v) TFA in acetonitrile. The flow rate was 0.8 mL/min from 0.01 to 1.51 min, then 1.2 mL/min from 1.52 to 2.00 min. The gradient ran from 90% mobile phase A to 10% mobile phase A over 1.15 min then remained at 10% mobile phase A through 1.65 min then back to 90% mobile phase A at 1.66 min and was maintained at 90% mobile phase A through 2.0 min. The UV detection was 220 nm and the MS was measured in positive ion mode.

Method B: Run on an Agilent 1200 with a MS 6120 detector using an Xbridge Shield RP18 column (2.1*50mm, 5um) at 40 °C. Mobile phase A was 10 mM aqueous NH_4HCO_3

and mobile phase B was acetonitrile. The flow rate was 1.0 mL/min from 0.01 to 2.48 min, then 1.2 mL/min from 2.50 to 3.00 min. The gradient ran from 90% mobile phase A to 20% mobile phase A over 2.00 min then remained at 20% mobile phase A through 2.48 min then back to 90% mobile phase A at 2.50 min and maintained at 90% mobile phase A through 3.0 min. The UV detection was 220 nm and the MS was measured in positive ion mode.

Method C: Run on an Agilent 1200 with a MS 6120 detector using an Xbridge Shield RP18 column (2.1*50mm, 5um) at 40 °C. Mobile phase A was 10 mM aqueous NH_4HCO_3 and mobile phase B was acetonitrile. The flow rate was 1.0 mL/min from 0.01 to 2.50 min, then 1.2 mL/min from 2.51 to 3.00 min. The gradient ran from 70% mobile phase A to 10% mobile phase A over 1.50 min then remained at 10% mobile phase A through 2.50 min then back to 70% mobile phase A at 2.51 min and maintained at 70% mobile phase A through 3.0 min. The UV detection was 220 nm and the MS was measured in positive ion mode.

Method D: Run on an Agilent 1200 with a MS 6120 detector using a Venusil XBP-C18 column (2.1*50mm, 5um) at 40 °C. Mobile phase A was 0.0375% aqueous TFA and mobile phase B was 0.018% TFA in acetonitrile. The flow rate was 0.8 mL/min from 0.01 to 4.5 min. The gradient was maintained at 99% mobile phase A from 0.00 min to 0.40 min, then the gradient ran from 99% mobile phase A to 10% mobile phase A over 3.00 min then to 0% mobile phase A over 0.45 min; then back to 99% mobile phase A over 0.01 min and maintained here for 0.55 min The UV detection was 220 nm and the MS was measured in positive ion mode.

Chemistry—The compounds in Figure 2, were sourced as follows. Compound **2** was prepared as described previously[34]. Pyrimethamine (**1**) was sourced from the drug manufacturer and ^{1}H NMR and LC/MS data confirmed structure and purity of 99.9%. Trimethoprim (**4**) was purchased from a commercial supplier as the lactate salt and ^{1}H NMR and LC/MS data confirmed structure with a purity of 98.7%. Methotrexate (**5**) was purchased from a commercial supplier and ^{1}H NMR and LC/MS data confirmed structure with a purity near 100%. Trimetrexate (**6**) was purchased from a commercial supplier as the tri-hydrochloride salt and ^{1}H NMR and LC/MS data confirmed structure with a purity of 95.2%.

The compounds in Tables 3, 4 and 5 were prepared according to Schemes 1 and 2.

Compounds **7–18** and **20 - 21** were prepared in a similar fashion as described below for the synthesis of **32**.

5-(4-(3-Bromophenyl)piperazin-1-yl)pyrimidine-2,4-diamine (**32**) was prepared in 3 steps and 12.8% overall yield as follows.

Step 1. *5-(4-([3-Bromophenyl])piperazin-1-yl)pyrimidine-2,4(1H,3H)-dione* **(37n).** To a mixture of 5-bromo-1H-pyrimidine-2,4-dione **33** (7.92 g, 42 mmol, 1.0 *eq*) and 1-(3-bromophenyl)piperazine **36n** (10.0 g, 42 mmol, 1.0 *eq*) in DMSO (200 mL) was added potassium fluoride (5.0 g, 94 mmol, 2.0 *eq*). The resulting mixture was stirred at 130°C for 12 h, cooled to room temperature and poured into 300 mL of water. The precipitate was

collected by suction filtration, washed with 200 mL of EtOH and dried in vacuo leaving 5-(4-([3-bromophenyl])piperazin-1-yl)pyrimidine-2,4(1H,3H)-dione **37n** as a brown solid (10.6 g, 30.2 mmol, 73.5% yield) used as such in the next step. LCMS Method B (ESI+): Expected m/z 351 $(M+1)^+$; found m/z 351 $(M+1)^+$, RT: 1.07 Min.

Step 2. *5-(4-(3-Bromophenyl)piperazin-1-yl)-2,4-dichloropyrimidine* **(38n).** A mixture of 5-(4-(3-bromophenyl)piperazin-1-yl)pyrimidine-2,4(1H,3H)-dione **37n** (10 g, 28.5 mmol, 1.0 *eq*) and DIPEA (14.4 g, 111 mmol, 3.9 eq) in 70 mL of toluene was cooled to 10 °C and $POCl_3$ (15.8 g, 103 mmol) was added over 1 h, keeping the reaction temperature 20°C. The mixture was stirred at 20°C for 1 h, heated to 95°C, and held at 95°C for 12 h. LCMS was consistent with the desired product MS. The reaction mixture was concentrated under reduced pressure to give a black residue, which was diluted with cold water (200 mL) and extracted with DCM (3 × 100 mL). The combined organic layers were washed with brine (2 × 100 mL), dried over Na_2SO_4, filtered and concentrated under reduced pressure to give 5-(4-(3-bromophenyl)piperazin-1-yl)-2,4-dichloropyrimidine (**38n**) (6.4 g, 58% yield, 90.8% HPLC purity) as a yellow solid used as such in the next step. LC/MS Method C (ESI+): Expected m/z 389.1 $(M+1)^+$; found m/z 389.0 $(M+1)^+$, RT: 2.18 Min.

Step 3. *5-(4-(3-Bromophenyl)piperazin-1-yl)pyrimidine-2,4-diamine (**32**).* A mixture of 5-(4-(bromophenyl)piperazin-1-yl)-2,4-dichloropyrimidine **38n** (100.0 mg, 0.26 mmol, 1.0 *eq*) in NH_3/EtOH (10 mL) was added to a steel bomb. The mixture was stirred at 145°C for 12 h. The suspension was cooled to room temperature and concentrated under reduced pressure to give a brown residue. The residue was purified by Prep-HPLC (TFA condition) to give 5-(4-(3-bromophenyl)piperazin-1-yl)pyrimidine-2,4-diamine **32** (86.5 mg, 249.6 μmol, 30.0% yield) as a white solid. LCMS Method D (ESI+): Expected m/z (349.0 and 351.1 $M+1)^+$; found m/z 349.0 and 351.1 $(M+1)^+$, Rt: 2.18 Min. ^{1}H NMR (DMSO-d_6 400MHz)) δ = 7.57 (s, 1H), 7.19 – 7.12 (m, 1H), 7.09 (br s, 1H), 6.94 (br dd, *J* = 7.9, 18.4 Hz, 2H), 5.65 (s, 2H), 3.29 (br s, 4H), 2.85 (br s, 4H).

5-(4-Phenylpiperazin-1-yl)pyrimidine-2,4-diamine (**7**) was prepared in an analogous 3 step manner as described for **32** starting with 1-phenylpiperazine (**36b**) to give a light yellow solid (26.6% yield). ^{1}H NMR (DMSO-d_6) δ = 7.59 (s, 1H), 7.22 (br t, *J*=7.8 Hz, 2H), 6.96 (br d, *J* = 8.2 Hz, 2H), 6.78 (t, *J* = 7.0 Hz, 1H), 6.07 (br s, 2H), 5.61 (br s, 2H), 3.25 (br s, 4H), 2.88 (br t, *J* = 4.5 Hz, 4H). LC/MS (M + 1) Expected MW 271.1, Observed MW 271.1, % UV purity 99.9%.

5-(4-([1,1'-Biphenyl]-2-yl)piperazin-1-yl)pyrimidine-2,4-diamine (**8**) was prepared in an analogous 3 step manner as described for **32** above starting with 1-([1,1'-biphenyl]-2-yl)piperazine (**36c**) to give **8** in 7.0% yield as a white solid. ^{1}H NMR (DMSO-d_6) δ = 7.65 (br d, *J* = 7.6 Hz, 2H), 7.48 (s, 1H), 7.44 (br t, *J* = 7.2 Hz, 2H), 7.31 (br t, *J* = 7.2 Hz, 2H), 7.21 (br d, *J* = 7.2 Hz, 1H), 7.12 – 7.05 (m, 2H), 5.99 (br s, 1H), 5.60 (s, 2H), 2.88 (br s, 4H), 2.64 (br s, 4H). LC/MS (M + 1) Expected MW 347.2, Observed MW 347.2, UV purity 97.8%.

5-(4-([1,1'-Biphenyl]-4-yl)piperazin-1-yl)pyrimidine-2,4-diamine (**9**) was prepared in an analogous 3 step manner as described for **32** starting with 1-([1,1'-biphenyl]-4-yl)piperazine

(**36d**) to give **9** in 10.6% yield as a white solid. ^{1}H NMR (METHANOL-d_4) δ = 7.60 – 7.50 (m, 5H), 7.39 (br t, *J* = 7.4 Hz, 2H), 7.30 – 7.23 (m, 1H), 7.10 (br d, *J* = 8.6 Hz, 2H), 3.48 – 3.36 (m, 4H), 3.03 (br d, *J* = 4.3 Hz, 4H). LC/MS (M + 1) Expected MW 347.2, Observed MW 347.2, UV Purity 96.7%.

5-(4-(*o*-Tolyl)piperazin-1-yl)pyrimidine-2,4-diamine (**10**) was prepared in an analogous 3 step manner as described for **32** starting with 1-(*o*-tolyl)piperazine (**36e**) to give **10** in 32.8% yield as a white solid. ^{1}H NMR (METHANOL-d_4) δ = 7.53 (s, 1H), 7.21 – 7.11 (m, 3H), 7.03 – 6.97 (m, 1H), 3.10 (br s, 4H), 3.03 (br d, *J* = 4.0 Hz, 4H), 2.34 (s, 3H). LC/MS (M + 1) Expected MW 285.2, Observed MW 285.1, UV Purity 99.4%.

5-(4-(*m*-Tolyl)piperazin-1-yl)pyrimidine-2,4-diamine (**11**) was prepared in an analogous 3 step manner as described for **32** starting with 1-(*m*-tolyl)piperazine (**36f**) to give **11** in 7.2% yield as a yellow solid. ^{1}H NMR (DMSO-d_6) δ = 7.59 (s, 1H), 7.10 (t, *J* = 7.8 Hz, 1H), 6.83 – 6.70 (m, 2H), 6.60 (br d, *J* = 7.4 Hz, 1H), 6.08 (br s, 2H), 5.62 (s, 2H), 3.23 (br s, 4H), 2.86 (br t, *J* = 4.3 Hz, 4H), 2.25 (s, 3H). LC/MS (M + 1) Expected MW 285.1, Observed MW 285.1, UV Purity 99.5%.

5-(4-(*p*-Tolyl)piperazin-1-yl)pyrimidine-2,4-diamine (**12**) was prepared in an analogous 3 step manner as described for **32** starting with 1-(*p*-tolyl)piperazine (**36g**) to give **12** in 2.3% yield as a white solid. ^{1}H NMR (DMSO-d_6) δ = 7.58 (s, 1H), 7.03 (d, *J* = 8.4 Hz, 2H), 6.86 (d, *J* = 8.4 Hz, 2H), 6.06 (br. s., 1H), 5.60 (s, 2H), 3.19 (br. s., 4H), 2.87 (d, *J* = 4.0 Hz, 4H), 2.20 (s, 3H). LC/MS (M + 1) Expected MW 285.1, Observed MW 285.1, UV Purity 98.1%.

5-(4-(2-Chlorophenyl)piperazin-1-yl)pyrimidine-2,4-diamine (**13**) was prepared in an analogous 3 step manner as described for **32** starting with 1-(2-chlorophenyl)piperazine (**36h**) to give **13** in 19.4% yield as a light yellow solid. ^{1}H NMR (DMSO-d_6) δ = 7.62 (s, 1H), 7.42 (br d, *J* = 7.8 Hz, 1H), 7.35 – 7.28 (m, 1H), 7.18 (br d, *J* = 7.8 Hz, 1H), 7.05 (br t, *J* = 7.4 Hz, 1H), 6.09 (br s, 2H), 5.63 (s, 2H), 3.11 (br s, 4H), 2.91 (br d, *J* = 3.9 Hz, 4H). LC/MS (M + 1) Expected MW 305.1, Observed MW 305.1, UV Purity 99.1%.

5-(4-(3-Chlorophenyl)piperazin-1-yl)pyrimidine-2,4-diamine (**14**) was prepared in an analogous 3 step manner as described for **32** starting with 1-(3-chlorophenyl)piperazine (**36i**) to give **14** in 6.6% yield as a solid. ^{1}H NMR (DMSO-d_6) δ = 11.76 (br, 1H), 8.43 (br s, 1H), 7.65 (br s, 1H), 7.56 (br s, 1H), 7.43 (br s, 2H), 7.23 (br t, *J* = 8.4 Hz, 1H), 6.98 (br s, 1H), 6.93 (br d, *J* = 8.4 Hz, 1H), 6.80 (br d, *J* = 7.6 Hz, 1H), 3.36 (br s, 4H), 2.86 (br s, 4H). LC/MS (M + 1) Expected MW 305.1, Observed MW 305.1, UV Purity 98.1%.

5-(4-(4-Chlorophenyl)piperazin-1-yl)pyrimidine-2,4-diamine (**15**) was prepared in an analogous 3 step manner as described for **32** starting with 1-(4-chlorophenyl)piperazine (**36j**) to give **15** in 71.9% yield as a white solid. ^{1}H NMR (DMSO-d_6) δ = 7.58 (s, 1H), 7.24 (br d, *J* = 9.0 Hz, 2H), 6.97 (br d, *J* = 9.0 Hz, 2H), 6.08 (br s, 1H), 5.61 (s, 2H), 3.26 (br s, 4H), 2.86 (br t, *J* = 4.3 Hz, 4H). LC/MS (M + 1) Expected MW 305.1, Observed MW 305.1, UV Purity 96.3%.

5-(4-(3-Methoxyphenyl)piperazin-1-yl)pyrimidine-2,4-diamine (**16**) was prepared in an analogous 3 step manner as described for **32** starting with 1-(3-methoxyphenyl)piperazine

(**36k**) to give **16** in 24.2% yield as a white solid. ^{1}H NMR (DMSO-d_6) δ = 7.58 (s, 1H), 7.11 (t, *J* = 8.4 Hz, 1H), 6.54 (br d, *J* = 8.0 Hz, 1H), 6.47 (s, 1H), 6.37 (br d, *J* = 8.0 Hz, 1H), 6.08 (br s, 1H), 5.61 (s, 2H), 3.72 (s, 3H), 3.25 (br s, 4H), 2.86 (br d, *J* = 4.0 Hz, 4H). LC/MS (M + 1) Expected MW 301.1, Observed MW 301.1, UV Purity 98.7%.

5-(4-(3-(Trifluoromethyl)phenyl)piperazin-1-yl)pyrimidine-2,4-diamine (**17**) was prepared in an analogous 3 step manner as described for **32** starting with 1-(3-trifluoromethylphenyl)piperazine (**36l**) to give **17** in 18.8% yield as a yellow solid. ^{1}H NMR (METHANOL-d_4) δ = 7.50 (s, 1H), 7.44 – 7.39 (m, 1H), 7.23 (br d, *J* = 8.8 Hz, 1H), 7.20 (br s, 1H), 7.10 (br d, *J* = 7.5 Hz, 1H), 3.40 (br s, 4H), 3.01 (br d, *J* = 4.4 Hz, 4H). LC/MS (M + 1) Expected MW 339.1, Observed MW 339.1, UV Purity 99.5%.

5-(4-(3-(Trifluoromethoxy)phenyl)piperazin-1-yl)pyrimidine-2,4-diamine (**18**) was prepared in an analogous 3 step manner as described for **32** starting with 1-(3-trifluoromethoxyphenyl)piperazine (**36m**) to give **18** in 22.7% yield as a yellow solid. ^{1}H NMR (METHANOL-d_4) δ = 7.49 (s, 1H), 7.31 (t, *J* = 8.2 Hz, 1H), 6.98 (d, *J* = 7.9 Hz, 1H), 6.84 (s, 1H), 6.72 (d, *J* = 7.9 Hz, 1H), 3.38 (s, 4H), 2.99 (s, 4H). LC/MS (M + 1) Expected MW 355.1, Observed MW 355.1, UV Purity 100%.

5-(4-([1,1'-Biphenyl]-3-yl)piperazin-1-yl)-6-methylpyrimidine-2,4-diamine (**20**) was prepared in an analogous 3 step manner as described for **32** starting with 1-([1,1'-biphenyl]-3-yl)piperazine (**36a**) and 5-bromo-6-methyluracil (**34**) to give **20** in 31.8% yield as a yellow solid. ^{1}H NMR (METHANOL-d_4) d = 7.64 – 7.57 (m, 2H), 7.51 – 7.28 (m, 5H), 7.20 (br d, *J* = 7.5 Hz, 1H), 7.09 (br d, *J* = 7.9 Hz, 1H), 3.66 (br d, *J* = 11.5 Hz, 2H), 3.45 – 3.35 (m, 2H), 3.26 – 3.16 (m, 2H), 3.03 (br d, *J* = 11.5 Hz, 2H), 2.38 (s, 3H). LC/MS (M + 1) Expected MW 361.2, Observed MW 361.1, UV Purity 95.9%.

5-(4-([1,1'-Biphenyl]-3-yl)piperazin-1-yl)-6-ethylpyrimidine-2,4-diamine (**21**) was prepared in an analogous 3 step manner as described for **32** starting with 1-([1,1'-biphenyl]-3-yl)piperazine (**36a**) and 5-bromo-6-ethyluracil (**35**) to give **21** in 71.4% yield as a yellow solid. ^{1}H NMR (METHANOL-d_4) δ = 7.61 (d, *J* = 7.2 Hz, 2H), 7.43 (d, *J* = 8.0 Hz, 4H), 7.36 (d, *J* = 6.4 Hz, 1H), 7.30 (d, *J* = 7.2 Hz, 1H), 7.18 (d, *J* = 7.2 Hz, 1H), 3.65 (d, *J* = 9.2 Hz, 2H), 3.44–3.31 (m, 4H), 3.12 (d, *J* = 8.8 Hz, 2H), 2.73 (d, *J* = 7.6 Hz, 2H), 1.33 (t, *J* = 6.8 Hz, 3H). LC/MS (M + 1) Expected MW 375.2, Observed MW 375.1, UV Purity 98.7%.

Compounds **3, 19, 23, 24, 26, 28** and **30–31** were prepared in a similar fashion as described below for the synthesis of **29**.

5-(4-(3-(2-methylpyrimidin-5-yl)phenyl)piperazin-1-yl)pyrimidine-2,4-diamine (29)

A mixture of 5-(4-(3-bromophenyl)piperazin-1-yl)pyrimidine-2,4-diamine **32** (1.0 g, 2.8 mmol, 1.0 *eq*), (2-methylpyrimidin-5-yl)boronic acid **39u** (395 mg, 2.8 mmol, 1.0 *eq*), Cs_2CO_3 (1.4 g, 4.3 mmol, 1.5 *eq*), $Pd(PPh_3)_4$ (165 mg, 143 μmol, 0.05 *eq*) in dioxane (32 mL) and H_2O (8.0 mL) was degassed and purged with N_2 3 times, and then stirred at 100°C for 12 h under N_2 atmosphere. Then it was stirred with silica S thiol Met at 20 °C, filtered and concentrated to give a residue. The residue was purified by prep-HPLC (TFA condition)

to give 5-(4-(3-(2-methylpyrimidin-5-yl)phenyl)piperazin-1-yl)pyrimidine-2,4-diamine **29** (1.2 g, 2.5 mmol, 88.0% yield) as a white solid. ^{1}H NMR, (METHANOL-d_4) δ = 8.93 (s, 2H), 7.51 (s, 1H), 7.41 (t, *J* = 7.8 Hz, 1H), 7.26 – 7.24 (m, 1H), 7.16 – 7.09 (m, 2H), 3.44 (br s, 4H), 3.02 (br t, *J* = 4.8 Hz, 4H), 2.73 (s, 3H). LCMS expected m/z 363.2 $(M+1)^+$; found m/z 363.1 $(M+1)^+$. UV purity 99.0%.

5-(4-(3-(2-Methoxypyrimidin-5-yl)phenyl)piperazin-1-yl)pyrimidine-2,4-diamine (**3**) was prepared in an analogous manner as described for **29** starting with **32** and 5-(2-methoxypyrimidinyl)boronic acid (**39o**) to give **3** in 92.8% yield as a light yellow solid. ^{1}H NMR (METHANOL-d_4) δ = 8.81 (s, 2H), 7.51 (s, 1H), 7.39 (br t, *J* = 7.6 Hz, 1H), 7.22 (br s, 1H), 7.14 – 7.07 (m, 2H), 4.06 (s, 3H), 3.44 (br s, 4H), 3.03 (br s, 4H). Elemental analysis for $C_{19}H_{22}N_8O$ + 0.15 H_2O: Theoretical C 59.83%, H 5.90%, N 29.39%. Found C 59.56%, H 5.83%, N 29.05%. LC/MS (M + 1) Expected MW 379.2, Observed MW 379.1, UV Purity 96.4%.

5-(4-(3-Cyclopropylphenyl)piperazin-1-yl)pyrimidine-2,4-diamine (**19**) was prepared in an analogous manner as described for **29** starting with **32** and cyclopropyl boronic acid (**39p**) to give **19** in 59.2% yield as solid. ^{1}H NMR (METHANOL-d_4) δ = 7.52 (br s, 1H), 7.20 (br d, *J* = 7.2 Hz, 1H), 6.97 – 6.83 (m, 2H), 6.73 (br s, 1H), 3.43 (br s, 4H), 3.06 (br s, 4H), 1.91 (br s, 1H), 0.96 (br d, *J* = 6.0 Hz, 2H), 0.68 (br s, 2H). LC/MS (M + 1) Expected MW 311.2, Observed MW 311.1, UV Purity 98.9%.

5-(4-(3-(Pyridin-3-yl)phenyl)piperazin-1-yl)pyrimidine-2,4-diamine (**23**) was prepared in an analogous manner as described for **29** starting with **32** and 3-pyridyl boronic acid (**39q**) to give **23** in 28.2% yield as a light yellow oil. ^{1}H NMR (METHANOL-d_4) δ = 9.08 (br s, 1H), 8.79 – 8.69 (m, 2H), 8.01 (br s, 1H), 7.52 (s, 1H), 7.49 – 7.44 (m, 1H), 7.36 (s, 1H), 7.24 (d, *J* = 7.6 Hz, 1H), 7.19 (dd, *J* = 2.0, 8.4 Hz, 1H), 3.48 (br s, 4H), 3.04 (br s, 4H). LC/MS (M + 1) Expected MW 348.2, Observed MW 348.2, UV Purity 98.2%.

5-(4-(3-(Pyridin-4-yl)phenyl)piperazin-1-yl)pyrimidine-2,4-diamine (**24**) was prepared in an analogous manner as described for **29** starting with **32** and 4-pyridyl boronic acid (**39r**) to give **24** in 11.5% yield. ^{1}H NMR (METHANOL-d_4) δ = 8.56 (br s, 2H), 7.73 – 7.62 (m, 3H), 7.39 (br d, *J* = 8.8 Hz, 1H), 7.33 (br s, 1H), 7.22 (br d, *J* = 7.2 Hz, 1H), 7.13 (br d, *J* = 7.6 Hz, 1H), 3.50 – 3.35 (m, 4H), 3.03 (br s, 4H). LC/MS (M + 1) Expected MW 348.2, Observed MW 348.2, UV Purity 95.3%.

5-(4-(3-(Pyrimidin-5-yl)phenyl)piperazin-1-yl)pyrimidine-2,4-diamine (**26**) was prepared in an analogous manner as described for **29** starting with **32** and 5-pyrimidinyl boronic acid (**39s**) to give **26** in 34.9% yield as a light yellow oil. ^{1}H NMR (METHANOL-d_4) δ = 9.14 (br s, 1H), 9.07 (br s, 2H), 7.52 (s, 1H), 7.49 – 7.42 (m, 1H), 7.34 (br s, 1H), 7.21 (br dd, *J* = 7.7, 18.7 Hz, 2H), 3.48 (br s, 4H), 3.05 (br s, 4H). LC/MS (M + 1) Expected MW 349.1, Observed MW 349.1, UV Purity 95.8%.

5-(4-(3-(Pyridazin-4-yl)phenyl)piperazin-1-yl)pyrimidine-2,4-diamine (**28**) was prepared in an analogous manner as described for **29** starting with **32** and 4-pyridazine-boronic acid pinacol ester (**39t**) to give **28** in 9.2% yield as a yellow solid. ^{1}H NMR (METHANOL-d_4) δ

= 9.59 (s, 1H), 9.25 (d, *J* = 5.3 Hz, 1H), 8.10 (dd, *J* = 2.4, 5.5 Hz, 1H), 7.55 – 7.41 (m, 3H), 7.34 (br d, *J* = 7.9 Hz, 1H), 7.22 (br d, *J* = 8.4 Hz, 1H), 3.48 (br s, 4H), 3.04 (br d, *J* = 4.4 Hz, 4H). LC/MS (M + 1) Expected MW 349.2, Observed MW 349.1, UV Purity 100%.

5-(4-(3-(2-(Trifluoromethyl)pyrimidin-5-yl)phenyl)piperazin-1-yl)pyrimidine-2,4-diamine (**30**) was prepared in an analogous manner as described for **29** starting with **32** and 5-(2-trifluoromethylpyrimidine)-boronic acid (**39v**) to give **30** in 27.3% yield as a yellow solid. ^{1}H NMR (METHANOL-d4) δ = 9.23 (s, 2H), 7.51 (s, 1H), 7.46 – 7.44 (m, 1H), 7.36 (s, 1H), 7.25 (d, *J* = 8.0 Hz, 1H), 7.18 (d, *J* = 6.4 Hz, 1H), 3.47 (br s, 4H), 3.03 (br s, 4H). LC/MS (M + 1) Expected MW 417.2, Observed MW 417.1, UV Purity 98.2%.

5-(4-(3-(2-Cyclopropylpyrimidin-5-yl)phenyl)piperazin-1-yl)pyrimidine-2,4-diamine (**31**) was prepared in an analogous manner as described for **29** starting with **32** and 5-(2-cyclopropylpyrimidine)-boronic acid (**39w**) to give **31** in 42.9% yield as a light yellow solid. ^{1}H NMR (METHANOL-d_4) δ = 8.89 (s, 2H), 7.52 (s, 1H), 7.43 – 7.41 (m, 1H), 7.28 (s, 1H), 7.19–7.13 (m, 2H), 3.46 (br s, 4H), 3.04 (br s, 4H), 2.30 – 2.25 (m, 1H), 1.17 – 1.15 (m, 4H). Expected MW 389.2, Observed MW 389.1, UV Purity 100%.

Compounds **25** and **27** were prepared in a fashion as described below for the synthesis of **22**.

5-(4-(3-(pyridin-2-yl)phenyl)piperazin-1-yl)pyrimidine-2,4-diamine (22)

A mixture of 5-(4-(3-bromophenyl)piperazin-1-yl)pyrimidine-2,4-diamine **32** (100.0 mg, 286.3 μmol, 1.0 *eq*), tributyl(pyridin-2-yl)stannane **40x** (106 mg, 286 μmol, 1 eq), $Pd_2(dba)_3$ (7.8 mg, 8.6 μmol, 0.03 eq), XPhos (23 mg, 49 μmol, 0.17 *eq*) in dioxane (8.0 mL) was degassed and purged with N_2 3 times. The mixture was stirred at 100 °C for 12 h under N_2 atmosphere, concentrated under reduced pressure and the residue was purified by prep-HPLC (TFA condition) to give 5-(4-(3-(pyridin-2-yl)phenyl)piperazin-1-yl)pyrimidine-2,4-diamine **22** (4.5 mg, 4.5% yield) as a yellow solid. LCMS Method D (ESI+): Expected m/z (348.2 M+1)$^+$; found m/z 348.1 (M+1)$^+$. ^{1}H NMR (CD_3OD-d_6) δ = 8.60 (br d, *J* = 4.9 Hz, 1H), 7.94 – 7.88 (m, 1H), 7.87 – 7.82 (m, 1H), 7.63 (s, 1H), 7.58 (s, 1H), 7.42 – 7.34 (m, 3H), 7.12 (br s, 1H), 3.39 (br d, *J* = 11.0 Hz, 4H), 3.03 (br t, *J* = 4.6 Hz, 4H).

5-(4-(3-(Pyrimidin-2-yl)phenyl)piperazin-1-yl)pyrimidine-2,4-diamine (**25**) was prepared in an analogous manner as described for **22** starting with **32** and tributyl(pyrimidin-2-yl)stannane (**40y**) to give **25** in 23.5% yield as a white solid. ^{1}H NMR ((METHANOL-d_4) δ = 8.85 (br s, 2H), 8.07 (br s, 1H), 7.92 (br d, *J* = 6.6 Hz, 1H), 7.52 (br s, 1H), 7.40 (br d, *J* = 13.7 Hz, 2H), 7.21 (br s, 1H), 3.46 (br s, 4H), 3.05 (br s, 4H). Expected MW 349.2, Observed MW 349.2, UV Purity 97.1%.

5-(4-(3-(Pyrazin-2-yl)phenyl)piperazin-1-yl)pyrimidine-2,4-diamine (**27**) was prepared in an analogous manner as described for **22** starting with **32** and tributyl(pyrazin-2-yl)stannane (**40z**) to give **27** in 50.1% yield as a light yellow solid. ^{1}H NMR (METHANOL-d_4) δ = 9.19 (s, 1H), 8.73 (s, 1H), 8.60 (br d, *J* = 2.0 Hz, 1H), 8.30 (s, 1H), 8.11 (br d, *J* = 7.6 Hz, 1H), 7.73 – 7.65 (m, 2H), 7.62 (s, 1H), 3.85 (br s, 4H), 3.30 – 3.26 (m, 4H). Expected MW 349.2, Observed MW 349.2, UV Purity 99.1%.

DHFR assay for human and T. gondii.—All compounds were tested in duplicate and replicated in at least 3 independent experiments. Human and *T. gondii* DHFR assays were run in parallel using the same stocks to optimize selectivity data. Key comparator compounds **1** (n =12 for human and *T. gondii*) and **3** (n = 16 for human and *T. gondii*) were tested in free base form on the same days for optimal comparison. The protein expression and purification protocol was adapted from a previously published procedure[33]. *T. gondii* TS-DHFR was sub-cloned into a PET15b plasmid and transformed into Escherichia coli BL21 competent cells. Overnight cultured bacteria were inoculated into a 1 L LB culture media at a ratio of 1:100 at 37 °C. Upon reaching an OD 600 nm of 0.7, protein expression was induced with 0.5 mM isopropyl β-D-thiogalactoside at 16 °C overnight. Cells were then pelleted (~4.6 g) and re-suspended in buffer A (25 mM Tris-HCl, pH 7.3, 100 mM NaCl, 1 mM EDTA), before lysis by sonication. MTX agarose beads (~1 mL) were added to the lysate, and the beads were subsequently washed 2X with buffer A (~10 mL) and 1X with buffer B (~10 mL – 25 mM Tris-HCl, pH 7.3, 1 M KCl, 1 mM EDTA) prior to elution with buffer C (~6 mL, 25 mM Tris-HCl, 10 mM DTT, 10% glycerol, 2 mM H2F). The eluent containing the purified enzyme was then concentrated and the protein was transferred, using a PD-MiniTrap G-25 column, to the final storage buffer (25 mM TrisHCl, 10mM DTT, 10% glycerol). Purified hDHFR was obtained commercially from Sigma Aldrich; Dihydrofolate Reductase human (Sigma D6566). The protein was confirmed by sequencing.

The diaphorase-coupled assay for DHFR activity was adapted from a previously published procedure[57]. Compounds were added as solutions of DMSO at 100X the desired concentration to purified enzyme (1 μg/mL) suspended in assay buffer (150 mM KCl, 8.9 mM ß-mercaptoethanol in 40.0 mM sodium phosphate at pH 7.4) in 384-well format (corning 3573). Following a 15 min incubation at 25 °C, solutions of NADPH (1.6 μM, Sigma N7505) and DHF (10 μM, Sigma D7006) in assay buffer were added sequentially. The plate was then incubated at 25 °C for an additional 60 min prior to the addition of diaphorase (10 U/mL) and resazurin (5 μM, Sigma R7017). After a final 10 min incubation at 25 °C, fluorescence was measured using an EnVision plate reader (531 nmEx/590 nmEm). IC_{50} values were determined from the raw fluorometric data by non-linear regression using Graphpad Prism.

Parasite strains and cell lines

Tachyzoites of *T. gondii* strains were grown in monolayers of human foreskin fibroblasts (HFF) (ATCC SCRC 1041) maintained in complete medium (DMEM containing 10% FBS, 2 mM L-glutamine, 10 mM HEPES and 10 μg/ml gentamicin in 35 mM $NaHCO_3$ solution), 37°C in 5% CO_2. Following natural egress, tachyzoites were purified in HBSS containing 10 mM HEPES, 0.1 mM EGTA and separated from host debris using 3.0 micro polycarbonate membrane filters, followed by centrifugation at 400*g*.

Cell-based parasite growth assays using β-galactosidase—This work was performed at Evotec in Manchester, UK. Parasite growth inhibition assays were conducted using the type I RH strain, 2F clone that expresses bacterial β-galactosidase (β-gal), as described previously[58]. Compounds dissolved in DMSO at 10 mM stocks were diluted in medium to two times final concentrations and added to an equal volume of medium

containing 5×10^2 parasites and incubated for 20 min. Mixtures of compounds (ranging from 10 μM to 0.01 nM) containing 0.1% (v/v) DMSO, or DMSO alone were added to monolayers of HFF cells grown in 96 well plates, centrifuged at 300 *g* for 5 min, and returned to culture at 37°C, 5% CO_2. The cells were preincubated for 2 h in the presence of parasites. Varying concentrations of drugs were added to each well (100 μL volumes containing 0.2% DMSO in D10 media) to give a final concentration range of 0.02 to 10 μM in 0.1% DMSO. The plates were centrifuged at 300G for 5 min at room temperature and then incubated at 37°C in 5% CO_2 for 72 h. At the end of the incubation period, the monolayer was lysed in 1% Triton X-100 and β-gal activity monitored using 1 mM chlorophenol red-β-D-galactopyranoside by absorption at 570 nm, as described previously[58]. Individual EC_{50} values were determined from three or more independent biological replicates and are reported as mean values.

Generation of firefly luciferase (FLUC) tagged strains

This work was performed at Washington University of St. Louis. Experiments were conducted with the ME49*Δhx*::FLUC strain of *T. gondii,* a transgenic line that expresses firefly luciferase (FLUC)[59]. To tag additional strains with FLUC, a reporter plasmid was created using a two-step Gibson Assembly approach. Fragment one was generated from PCR linearized pUPRT::Floxed DHFR-TS* plasmid (Addgene #100606) that includes both 5' and 3' uracil phosphoribosyltransferase (UPRT) flanking regions to drive locus specific integration at the *UPRT* gene and a floxed *T. gondii* DHFR selectable marker. Fragment two was synthesized using a gBlock (IDT DNA) containing the constitutive *T. gondii* alpha-tubulin promoter (608-bp) driving expression of the firefly luciferase reporter (1641-bp). The expression construct was targeted to the *UPRT* gene in *T. gondii* by co-transfection with the CRISPR plasmid pSAG1:CAS9, U6:sgUPRT. Parasites were sequentially selected in pyrimethamine (1.0 μM) followed by 5-fluorodeoxyracil (FUDR, 10 μM) and independent clones isolated by limiting dilution. All clones contain the floxed *T.gondii* DHFR selectable marker that can be excised using a plasmid expressing CRE recombinase.

In vitro growth assays using luciferase

To assess potency of compounds on different strains of *T. gondii*, values were determined form a 10-point dose-response curve. Briefly, 5×10^3 of luciferase expressing parasites (100 μL/well) were added to a 96-well plate that contained 100 μL of 2X compound concentration (to achieve 1X final compound concentration in 200 μL total well volume containing 0.1% DMSO) and allowed to replicate for 72 h prior to preparation for luciferase assay. All experimental steps, growth conditions and luciferase assay protocols were completed as described above. Compounds were tested using a 3-fold dilution series from 10 μM to 0.001 μM with all wells containing a final concentration of 0.1% DMSO. The EC_{50} data are presented as the average of three or more biological replicates (i.e. separate EC_{50} titrations) each with two technical replicates (i.e. separate wells).

Antiproliferative assay in MCF7 cells—This work was performed at Cyprotex in Watertown, MA. MCF-7 cells were plated on 96-well tissue culture treated polystyrene plates at 0.75×104 cells in 100 μL of MEM/EBSS (supplemented with 10% fetal bovine serum, sodium pyruvate, and antibiotics) per well. After an overnight incubation at 37°C, the

cells were dosed with test compounds and controls at a range of concentrations and incubated for 72 h at 37°C. Pyrimethamine **1** was tested from 0.156 to 20 μM and Compound **3** was evaluated from 0.313 to 40 μM with an 8-point dose curve in triplicate on three separate plates. Cell viability was measured using the Promega CellTiter 96 Non-Radioactive Cell Proliferation Assay (MTT) kit by adding 15 μL of the Dye Solution to each well and incubating for 3 h at 37°C. After incubation, 100 μL of the Solubilization Solution/ Stop Mix was added to each well. Plates were incubated at 37°C for 1 h, mixed on a plate shaker for 10 min and then absorbance was read at 570 nm. The EC_{50} was then calculated.

Pharmacokinetics (mouse)—Fasted female CD-1 mice (n = 3), 6–8 weeks old (supplied from Beijing Vital River Laboratory Animal Technology Co., Ltd) were administered a 0.5 mg/kg intravenous dose of compound **3**, formulated as a clear 0.1 mg/mL solution in saline at pH 5. A second group (n=3) was administered a 0.83 mg/kg oral dose of compound **3** (targeted dose was 1.0 mg/kg), formulated as a 0.1 mg/mL homogenous opaque suspension with fine particles in 0.5% CMC. Plasma (EDTA-K_2) from the iv dose was collected at 0.083, 0.50, 1.0, 2.0, 4.0, 8.0 and 24 h. Plasma (EDTA-K_2) from the po dose was collected at 0.50, 1.0, 2.0, 4.0, 8.0, 12 and 24 h. Plasma preparation: An aliquot of 10 μL plasma was protein precipitated with 100 μL IS, the mixture was vortexed and centrifuged at 13000 rpm for 10 min, 4°C. The supernatant (25 μL) was then mixed with 25 μL water/ACN (v:v, 95:5) containing 0.1% formic acid, vortexed and centrifuged at 4 °C, 3 μL of supernatant was injected for LC-MS/MS analysis. Concentration of compound **3** was determined using an LC-MS/MS-AG (API 4000) instrument in ESI positive mode with SRM detection monitoring for $[M+H]^+$ m/z transition 379.3/152.2 and using an internal standard 100 ng/mL tolbutamide $[M+H]^+$ m/z transition 271.1/155.1. The UPLC method Mobile Phase A: 0.025% formic acid, 1 mM NH4OAc in water/ACN (v:v, 95:5) and Mobile Phase B: 0.025% formic acid, 1 mM NH4OAc in ACN/water (v:v, 95:5) used a gradient starting with 15% Mobile Phase B and going to 90% over 1.40 min, on a Acquity UPLC BEH C18 1.7 μm 2.1 × 50 mm column at 60 °C at a flow rate of 0.7 mL/min. The retention time of compound **3** was 0.55 min and tolbutamide 0.88 min. A calibration curve from 1.00 to 3000 ng/mL of compound **3** in male CD-1 mouse plasma (EDTA-K_2) was made and the data analyzed using Phoenix WinNonlin 6.3 with a linear/log trapezoidal calculation method.

Brain to blood ratio (mouse)—This work was performed at Evotec, Manchester, UK. Fed, female CD1 mice (n = 3) were orally administered 10 mg/kg of the TFA-salt form of compound **3**, formulated as a clear solution in 0.25% carboxymethyl cellulose (CMC). Blood (EDTA-K_2) 20 μL was collected by tail prick of the lateral tail vein 0.5 h post-dose and diluted 2x with water for LC-MS/MS injection. Animals were then euthanized, and brain was collected and homogenized. The brain homogenates (40 μl) were run within the blood calibration curve and utilized the homogenization dilution factors for final quantitation but also incorporated a 2-fold adjustment for sample volume versus blood.

In vivo murine model of Toxoplasmosis

This work was performed at Evotec in Manchester, UK. Fed female CD-1 mice (60 mice per study; 12 mice per drug treatment group, 9 mice for vehicle and 3 mice as negative controls) were inoculated intraperitoneally with 3,000 tachyzoites of the highly virulent RH strain of

T. gondii on Day 0. The *T. gondii* strain used in this study had been genetically modified to constitutively express the enzyme fire fly luciferase (FLUC) and enable infection monitoring via an in vivo bioluminescence imaging system[53]. Beginning 24 h after inoculation, mice were dosed with either compound **1** formulated at 0.6, 1.8 and 5.4 mg/mL in 0.25% CMC or the TFA salt form of compound **3** formulated in 0.25% CMC at 0.1 mg/mL, 0.3 mg/mL or 1.0 mg/mL as a clear solution and dosed at a volume of 10 mL/kg. On day 4 micro-sampling of blood from the tail vein was collected into K2EDTA tubes and evaluated by LC/MS-MS as described above for the mouse brain to blood experiment.

Supplementary Material

Refer to Web version on PubMed Central for supplementary material.

Acknowledgement:

The authors are grateful to Rubin Ben-Harari and Nick Pelliccione for their contributions to the writing of this manuscript and support. The authors are also grateful to the chemists, in vitro pharmacologists and ADME/DMPK personal at WuXi for generating much of lead optimization data summarized in this paper.

Funding source: This study was funded by Vyera Pharmaceuticals. Contributions on this project from Dr. Sibley's laboratory were supported by a research Agreement between Vyera Pharmaceuticals and Washington University.

Abbreviations (nonstandard) used:

FLUC	fire fly luciferase
CMC	carboxymethyl cellulose
UPRT	uracil phosphoribosyltransferase
DHFR	Dihydrofolate reductase
CNS	central nervous system
MTX	methotrexate
HFF	human foreskin fibroblasts

REFERENCES:

1. Dubey JP; Lindsay DS; Speer CA, Structures of Toxoplasma gondii tachyzoites, bradyzoites, and sporozoites and biology and development of tissue cysts. Clin Microbiol Rev 1998, 11 (2), 267–299. [PubMed: 9564564]
2. Tenter AM; Heckeroth AR; Weiss LM, Toxoplasma gondii: from animals to humans. Int J Parasitol 2000, 30 (12–13), 1217–1258. [PubMed: 11113252]
3. Jones JL; Kruszon-Moran D; Rivera HN; Price C; Wilkins PP, Toxoplasma gondii seroprevalence in the United States 2009–2010 and comparison with the past two decades. Am J Trop Med Hyg 2014, 90 (6), 1135–1139. [PubMed: 24710615]
4. Maenz M; Schluter D; Liesenfeld O; Schares G; Gross U; Pleyer U, Ocular toxoplasmosis past, present and new aspects of an old disease. Progress in retinal and eye research 2014, 39, 77–106. [PubMed: 24412517]

5. Pappas G; Roussos N; Falagas ME, Toxoplasmosis snapshots: global status of Toxoplasma gondii seroprevalence and implications for pregnancy and congenital toxoplasmosis. Int J Parasitol 2009, 39 (12), 1385–1394. [PubMed: 19433092]
6. Prusa A-R; Kasper DC; Sawers L; Walter E; Hayde M; Stillwaggon E, Congenital toxoplasmosis in Austria: Prenatal screening for prevention is cost-saving. PLoS Negl Trop Dis 2017, 11 (7), e0005648. [PubMed: 28692640]
7. Dalimi A; Abdoli A, Latent toxoplasmosis and human. Iran J Parasitol 2012, 7 (1), 1–17.
8. Montoya A; Boothroyd JC; Kovacs J, Toxoplasma gondii In Mandell, Douglas, and Bennett's Principles and Practice of Infectious Diseases, 8th ed.; Elsevier Saunders: Philadelphia, PA, 2015; pp 3122–3153.
9. Halonen SK; Weiss LM, Chapter 8 - Toxoplasmosis In Handbook of clinical neurology, Hector H. Garcia HBT; Oscar HDB, Eds. Elsevier: 2013; Vol. Volume 114, pp 125–145. [PubMed: 23829904]
10. Rabaud C; May T; Amiel C; Katlama C; Leport C; Ambroise-Thomas P; Canton P, Extracerebral toxoplasmosis in patients infected with HIV. A French National Survey. Medicine (Baltimore) 1994, 73 (6), 306–14. [PubMed: 7984082]
11. Akira S, The role of IL-18 in innate immunity. Current Opinion in Immunology 2000, 12, 59–63. [PubMed: 10679398]
12. Cuervo G; Simonetti AF; Alegre O; Sanchez-Salado JC; Podzamczer D, Toxoplasma myocarditis: a rare but serious complication in an HIV-infected late presenter. Aids 2016, 30 (14), 2253–4. [PubMed: 27574795]
13. Cuervo G; Simonetti AF; Alegre O; Sanchez-Salado JC; Podzamczer D, Toxoplasma myocarditis: a rare but serious complication in an HIV-infected late presenter. AIDS 2016, 30 (14), 2253–2254. [PubMed: 27574795]
14. Montoya JG; Liesenfeld O, Toxoplasmosis. Lancet 2004, 363 (9425), 1965–1976. [PubMed: 15194258]
15. Olliaro P, Drug resistance hampers our capacity to roll back malaria. Clin Infect Dis 2005, 41 Suppl 4, S247–57. [PubMed: 16032560]
16. McCabe RE, Antitoxoplasma chemotherapy In Toxoplasmosis: a comprehensive clinical guide, Joynson DHM; Wreghitt TG, Eds. Cambridge Univ. Press: Cambridge, 2001; pp 319–359.
17. Ben-Harari RR; Goodwin E; Casoy J, Adverse Event Profile of Pyrimethamine-Based Therapy in Toxoplasmosis: A Systematic Review. Drugs R D 2017, 17 (4), 523–544. [PubMed: 28879584]
18. Khan Assir MZ; Ahmad HI; Akram J; Yusuf NW; Kamran U, An Outbreak of Pyrimethamine Toxicity in Patients with Ischaemic Heart Disease in Pakistan. Basic & Clinical Pharmacology & Toxicology 2014, 115 (3), 291–296. [PubMed: 24490639]
19. Eyles DE; Coleman N, Tests of 2,4-diaminopyrimidines on toxoplasmosis. Public Health Rep. 1952, 67, 249–52. [PubMed: 14900360]
20. Felix JPF; Lira RPC; Zacchia RS; Toribio JM; Nascimento MA; Arieta CEL, Trimethoprim-Sulfamethoxazole Versus Placebo to Reduce the Risk of Recurrences of Toxoplasma Gondii Retinochoroiditis: Randomized Controlled Clinical Trial. American Journal of Ophthalmology 2014, 157 (4), 762–766.e1. [PubMed: 24388839]
21. Stanford MR; See SE; Jones LV; Gilbert RE, Antibiotics for toxoplasmic retinochoroiditis: an evidence-based systematic review. Ophthalmology 2003, 110 (5), 926–31; quiz 931–2. [PubMed: 12750091]
22. Taques IIGG; Barbosa TR; Martini A. d. C.; Pitchenin LC; Braga ÍA; de Melo ALT; Nakazato L; Dutra V; de Aguiar DM, Molecular assessment of the transplacental transmission of Toxoplasma gondii, Neospora caninum, Brucella canis and Ehrlichia canis in dogs. Comparative immunology, microbiology and infectious diseases 2016, 49, 47–50.
23. Peters PJ; Thigpen MC; Parise ME; Newman RD, Safety and toxicity of sulfadoxine/pyrimethamine implications for malaria prevention in pregnancy using intermittent preventive treatment. Drug Saf. 2007, 30 (6), 481–501. [PubMed: 17536875]
24. Carr A; Cooper DA; Penny R, Allergic manifestations of human immunodeficiency virus (HIV) infection. J Clin Immunol 1991, 11 (2), 55–64. [PubMed: 1676034]
25. Phillips E; Mallal S, Drug hypersensitivity in HIV. Curr Opin Allergy Clin Immunol 2007, 7 (4), 324–30. [PubMed: 17620824]

26. Slatore CG; Tilles SA, Sulfonamide hypersensitivity. Immunol Allergy Clin North Am 2004, 24 (3), 477–90, vii. [PubMed: 15242722]
27. Amabeoku G; Chikuni O, GABAergic and dopaminergic systems may be involved in seizures induced by pyrimethamine in mice. Gen. Pharmacol 1994, 25 (6), 1269–77. [PubMed: 7875556]
28. Bolstad DB; Bolstad ESD; Frey KM; Wright DL; Anderson AC, Structure-Based Approach to the Development of Potent and Selective Inhibitors of Dihydrofolate Reductase from Cryptosporidium. J. Med. Chem 2008, 51 (21), 6839–6852. [PubMed: 18834108]
29. Chan DCM; Fu H; Forsch RA; Queener SF; Rosowsky A, Design, synthesis, and antifolate activity of new analogues of piritrexim and other diaminopyrimidine dihydrofolate reductase inhibitors with ω-carboxyalkoxy or ω-carboxy-1-alkynyl substitution in the side chain. J. Med. Chem 2005, 48 (13), 4420–4431. [PubMed: 15974594]
30. Jackson HC; Biggadike K; McKilligin E; Kinsman OS; Queener SF; Lane A; Smith J, 6,7-Disubstituted 2,4-diaminopteridines: novel inhibitors of Pneumocystis carinii and Toxoplasma gondii dihydrofolate reductase. Antimicrob. Agents Chemother 1996, 40 (6), 1371–1375. [PubMed: 8726003]
31. Pelphrey PM; Popov VM; Joska TM; Beierlein JM; Bolstad ESD; Fillingham YA; Wright DL; Anderson AC, Highly efficient ligands for dihydrofolate reductase from cryptosporidium hominis and toxoplasma gondii inspired by structural analysis. J. Med. Chem 2007, 50 (5), 940–950. [PubMed: 17269758]
32. Rosowsky A; Hynes JB; Queener SF, Structure-activity and structure-selectivity studies on diaminoquinazolines and other inhibitors of Pneumocystis carinii and Toxoplasma gondii dihydrofolate reductase. Antimicrob. Agents Chemother. 1995, 39 (1), 79–86. [PubMed: 7695334]
33. Sharma H; Landau MJ; Vargo MA; Spasov KA; Anderson KS, First Three-Dimensional Structure of Toxoplasma gondii Thymidylate Synthase-Dihydrofolate Reductase: Insights for Catalysis, Interdomain Interactions, and Substrate Channeling. Biochemistry 2013, 52 (41), 7305–7317. [PubMed: 24053355]
34. Welsch ME; Zhou J; Gao Y; Yan Y; Porter G; Agnihotri G; Li Y; Lu H; Chen Z; Thomas SB, Discovery of Potent and Selective Leads against Toxoplasma gondii Dihydrofolate Reductase via Structure-Based Design. *ACS Med*. Chem. Lett 2016, 7 (12), 1124–1129.
35. Allegra CJ; Kovacs JA; Drake JC; Swan JC; Chabner BA; Masur H, Potent in vitro and in vivo antitoxoplasma activity of the lipid-soluble antifolate trimetrexate. J. Clin. Invest 1987, 79 (2), 478–82. [PubMed: 2948969]
36. Gomes TC; de AJHF; Lescano SAZ; Amato-Neto V, In vitro action of antiparasitic drugs, especially artesunate, against Toxoplasma gondii. Rev Soc Bras Med Trop 2012, 45 (4), 485–90. [PubMed: 22930046]
37. Gao R; Canney DJ, A Versatile and Practical Microwave-Assisted Synthesis of Sterically Hindered N-Arylpiperazines. J. Org. Chem 2010, 75 (21), 7451–7453. [PubMed: 20863109]
38. Ravilla L; Venkata Subba Naidu N; Nagarajan K, An efficient scale up process for synthesis of N-arylpiperazines. Tetrahedron Lett. 2015, 56 (30), 4541–4544.
39. Lamb KM; G-Dayanandan N; Wright DL; Anderson AC, Elucidating Features That Drive the Design of Selective Antifolates Using Crystal Structures of Human Dihydrofolate Reductase. Biochemistry 2013, 52 (41), 7318–7326. [PubMed: 24053334]
40. UniProtKB, U. UniProtKB-P00374 (DYR_HUMAN) [database entry for human DHFR]. (accessed November 2, 2017).
41. Su CL; Khan A; Zhou P; Majumdar D; Ajzenberg D; Dardé ML; Zhu XQ; Ajioka JW; Rosenthal B; Dubey JP; Sibley LD, Globally diverse *Toxoplasma gondii* isolates comprise six major clades originating from a small number of distinct ancestral lineages. Proc. Natl. Acad. Sci. (USA) 2012, 109, 5844–5849. [PubMed: 22431627]
42. Ajzenberg D; Cogné N; Paris L; Bessieres MH; Thulliez P; Fillisetti D; Pelloux H; Marty P; Dardé ML, Genotype of 86 *Toxoplasma gondii* isolates associated with human congenital toxoplasmosis and correlation with clinical findings. J. Infect. Dis 2002, 186, 684–689. [PubMed: 12195356]
43. Ajzenberg D; Yera H; Marty P; Paris L; Dalle F; Menotti J; Aubert D; Franck J; Bessieres MH; Quinio D; Pelloux H; Delhaes L; Desbois N; Thulliez P; Robert-Gangneux F; Kauffmann-Lacroix C; Pujol S; Rabodonirina M; Bougnoux ME; Cuisenier B; Duhamel C; Duong TH; Filisetti D;

Flori P; Gay-Andrieu F; Pratlong F; Nevez G; Totet A; Carme B; Bonnabau H; Darde ML; Villena I, Genotype of 88 *Toxoplasma gondii* isolates associated with toxoplasmosis in immunocompromised patients and correlation with clinical findings. J Infect Dis 2009, 199 (8), 1155–67. [PubMed: 19265484]

44. Howe DK; Sibley LD, *Toxoplasma gondii* comprises three clonal lineages: correlation of parasite genotype with human disease. J. Infect. Dis 1995, 172, 1561–1566. [PubMed: 7594717]
45. Lunde MN; Jacobs L, Antigenic differences between endozoites and cystozoites of *Toxoplasma gondii*. Journal of Parasitology 1983, 65, 806–808.
46. Khan A; Su C; German M; Storch GA; Clifford D; Sibley LD, Genotyping of Toxoplasma gondii strains from immunocompromised patients reveals high prevalence of type I strains. J. Clin. Micro 2005, 43, 5881–5887.
47. Su C; Howe DK; Dubey JP; Ajioka JW; Sibley LD, Identification of quantitative trait loci controlling acute virulence in *Toxoplasma gondii*. Proc. Natl. Acad. Sci. (USA) 2002, 99, 10753–10758. [PubMed: 12149482]
48. Dubey J, Mouse pathogenicity of *Toxoplasma gondii* isolated from a goat. American Journal of Veterinary Research 1980, 41, 427–429. [PubMed: 7369619]
49. Carme B; Bissuel F; Ajzenberg D; Bouyne R; Aznar C; Demar M; Bichat S; Louvel D; Bourbigot AM; Peneau C; Neron P; Dardé ML, Severe acquired toxoplasmsis in immunocompetent adult patients in French Guiana. J . Clin. Microbiol 2002, 40, 4037–4044. [PubMed: 12409371]
50. Demar M; Hommel D; Djossou F; Peneau C; Boukhari R; Louvel D; Bourbigot AM; Nasser V; Ajzenberg D; Darde ML; Carme B, Acute toxoplasmoses in immunocompetent patients hospitalized in an intensive care unit in French Guiana. Clin Microbiol Infect 2012, 18 (7), E221–31. [PubMed: 21958195]
51. Lorenzi H; Khan A; Behnke MS; Namasivayam S; Swapna LS; Hadjithomas M; Karamycheva S; Pinney D; Brunk BP; Ajioka JW; Ajzenberg D; Boothroyd JC; Boyle JP; Darde ML; Diaz-Miranda MA; Dubey JP; Fritz HM; Gennari SM; Gregory BD; Kim K; Saeij JP; Su C; White MW; Zhu XQ; Howe DK; Rosenthal BM; Grigg ME; Parkinson J; Liu L; Kissinger JC; Roos DS; Sibley LD, Local admixture of amplified and diversified secreted pathogenesis determinants shapes mosaic Toxoplasma gondii genomes. Nat Commun 2016, 7, 10147. [PubMed: 26738725]
52. Reynolds MG; Roos DS, A biochemical and genetic model for parasite resistance to antifolates. Toxoplasma gondii provides insights into pyrimethamine and cycloguanil resistance in Plasmodium falciparum. J Biol Chem 1998, 273 (6), 3461–9. [PubMed: 9452469]
53. Behnke MS; Fentress SJ; Mashayekhi M; Li LL; Taylor GA; L.D. S, The polymorphic pseudokinase ROP5 controls virulence in Toxoplasma gondii by regulating the active kinase ROP18. PLoS Path. 2012, 8, e1002992.
54. Arribas JR; de Diego JA; Gamallo C; Vazquez JJ, A new murine model of severe acute toxoplasma encephalitis. J. Antimicrob. Chemother 1995, 36 (3), 503. [PubMed: 8830014]
55. Martins-Duarte ES; de Souza W; Vommaro RC, Toxoplasma gondii: The effect of fluconazole combined with sulfadiazine and pyrimethamine against acute toxoplasmosis in murine model. Exp. Parasitol 2013, 133 (3), 294–299. [PubMed: 23270807]
56. Piketty C; Derouin F; Rouveix B; Pocidalo JJ, In vivo assessment of antimicrobial agents against toxoplasma gondii by quantification of parasites in the blood, lungs, and brain of infected mice. Antimicrob. Agents Chemother. 1990, 34 (8), 1467. [PubMed: 2221854]
57. Kumar A; Zhang M; Zhu L; Liao RP; Mutai C; Hafsat S; Sherman DR; Wang M-W, High-throughput screening and sensitized bacteria identify an M. tuberculosis dihydrofolate reductase inhibitor with whole cell activity. PLoS One 2012, 7 (6), e39961. [PubMed: 22768185]
58. Lourido S; Zhang C; Lopez MS; Tang K; Barks J; Wang Q; Wildman SA; Shokat KM; Sibley LD, Optimizing small molecule inhibitors of calcium-dependent protein kinase 1 to prevent infection by *Toxoplasma gondii*. J. Med. Chem 2013, 56, 3068–3077. [PubMed: 23470217]
59. Tobin CM; Knoll LJ, A patatin-like protein protects Toxoplasma gondii from degradation in a nitric oxide-dependent manner. Infect. Immun 2012, 80 (1), 55–61. [PubMed: 22006568]

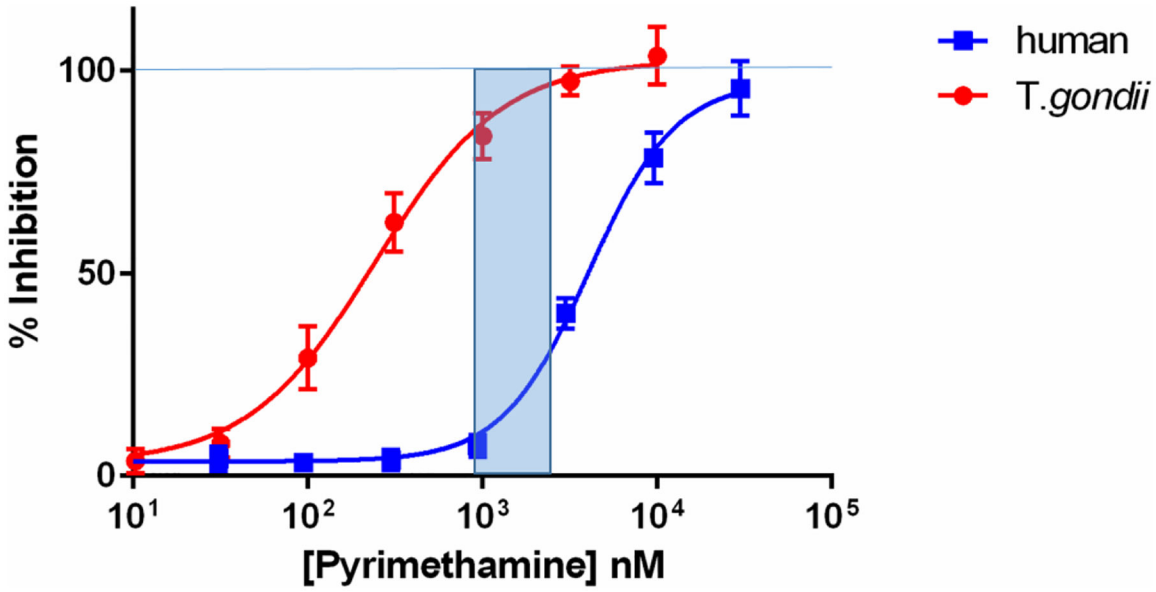

Figure 1.

[a]Dose response curve of **1** for inhibition of *T. gondii* DHFR and *human* DHFR

[a]The shaded blue area represents the concentration of **1** with >80% inhibition of *Tg*DHFR and 5 to 35% *h*DHFR.

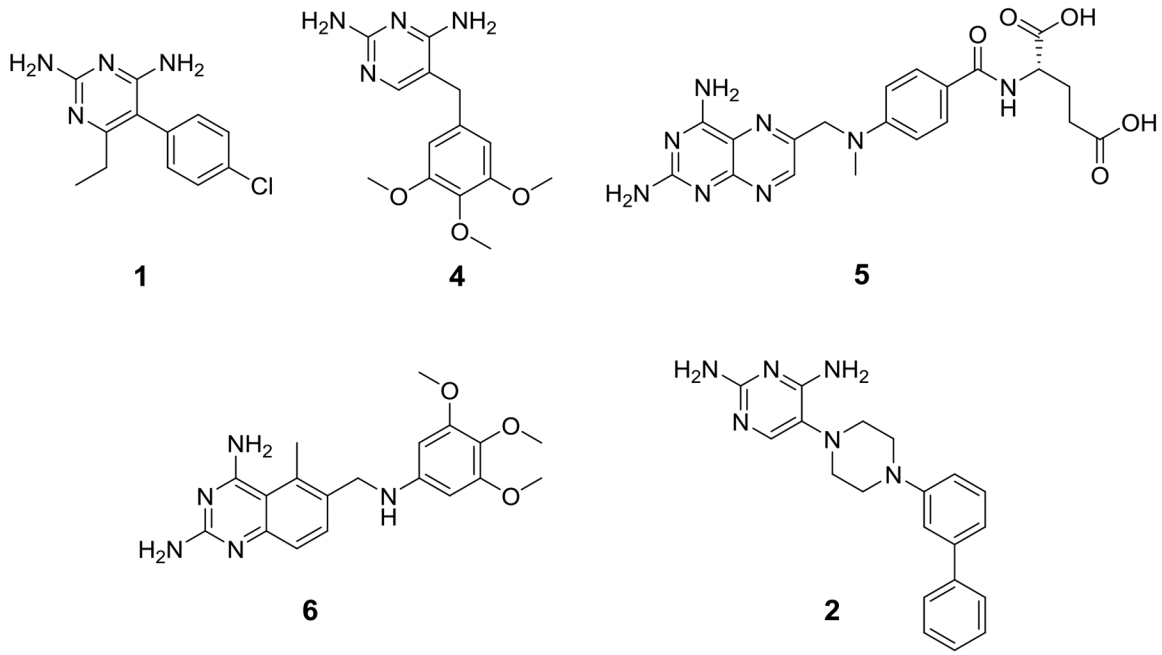

Figure 2.

Reference compounds Pyrimethamine (**1**), Trimethoprim (**4**), Methotrexate (**5**), Trimetrexate (**6**) and initial lead TRC-19 (**2**).

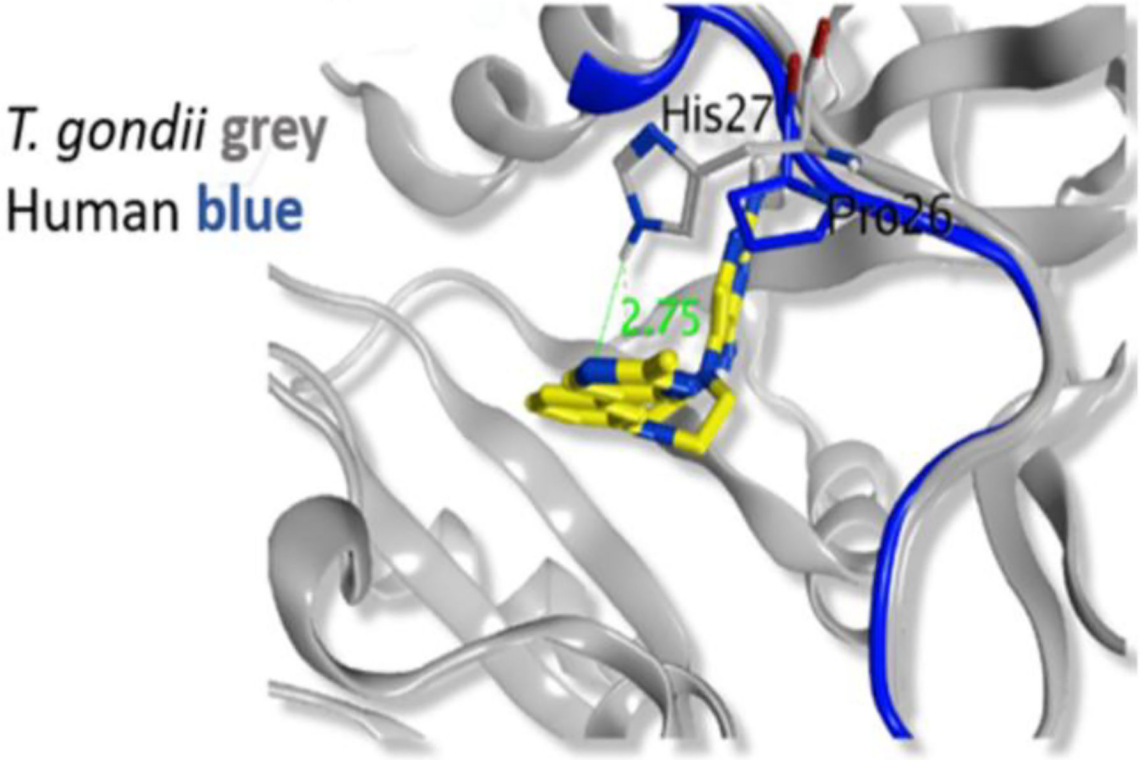

Figure 3.

Crystal Structure of *Tg*DHFR with pyrimidines **29** and **3** bound.

Crystal structure data was visualized and modeled using MOE software from Chemical Consulting Group.

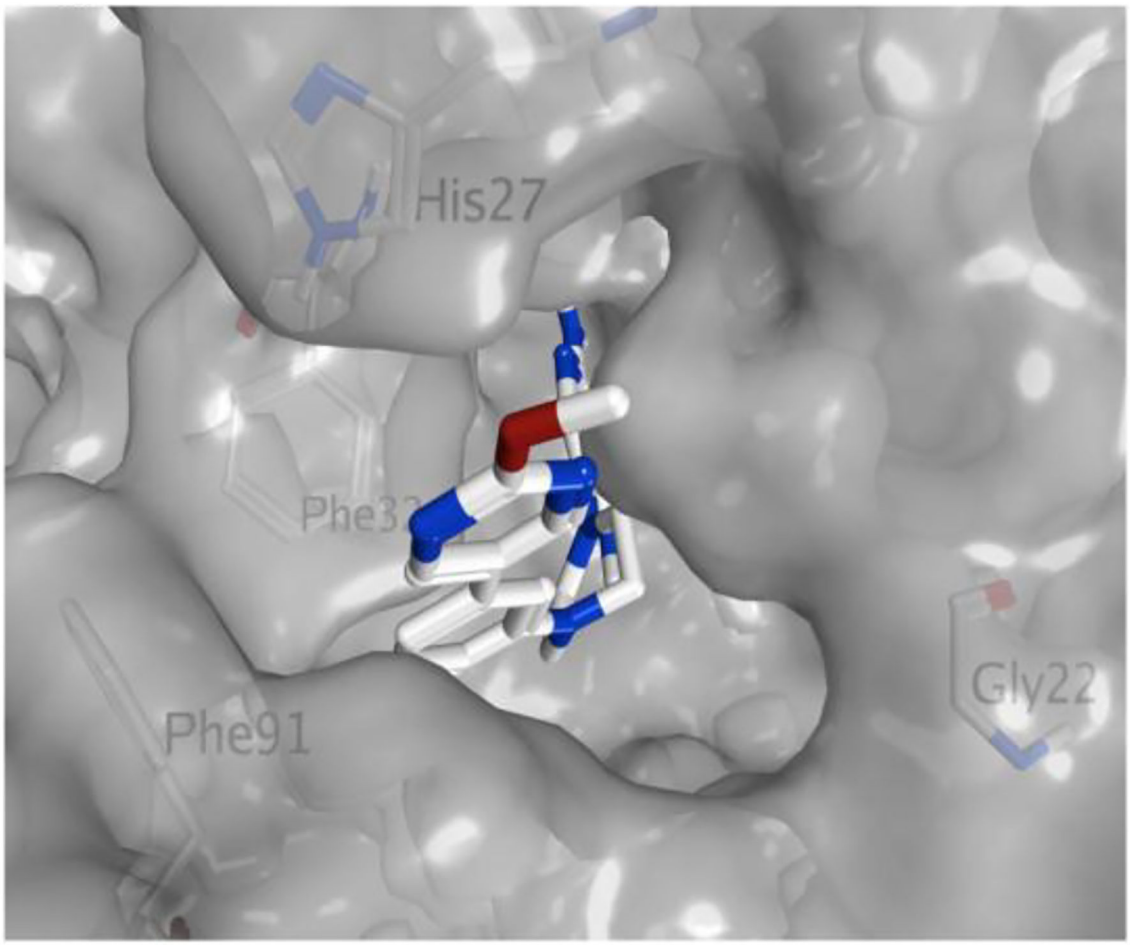

Figure 4.

Crystal Structure of *Tg*DHFR with pyrimidines **29** and **3** bound.

Crystal structure data was visualized and modeled using MOE software from Chemical Consulting Group.

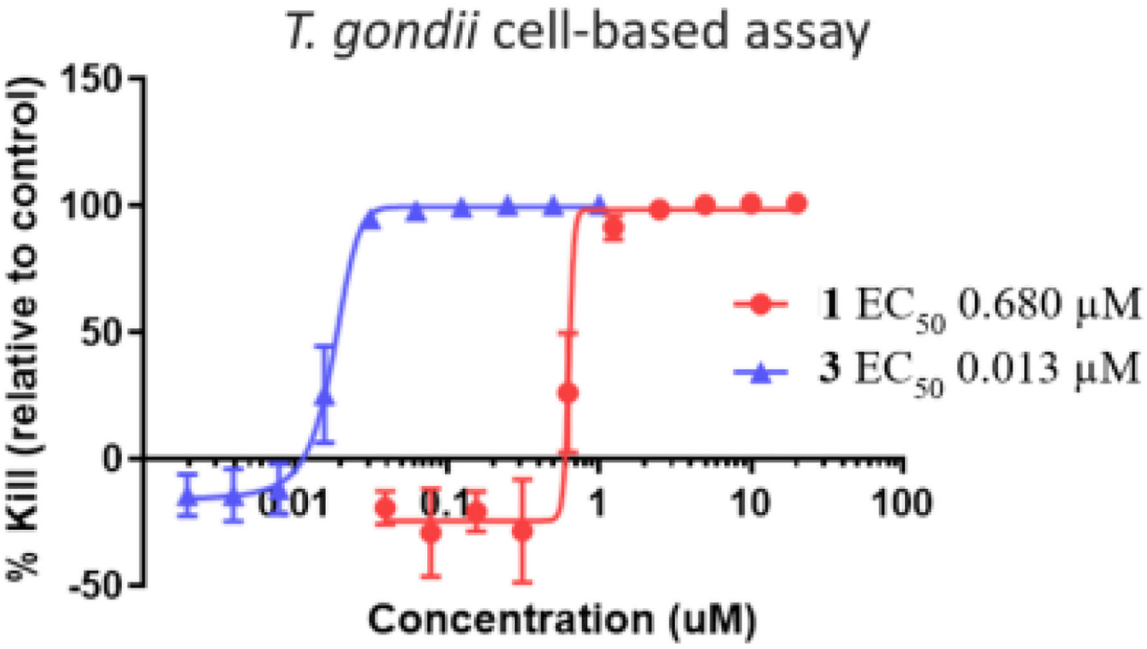

Figure 5.
Parasiticidal dose response curves of **1** and **3** in *T. gondii* infected human foreskin fibroblast cells.

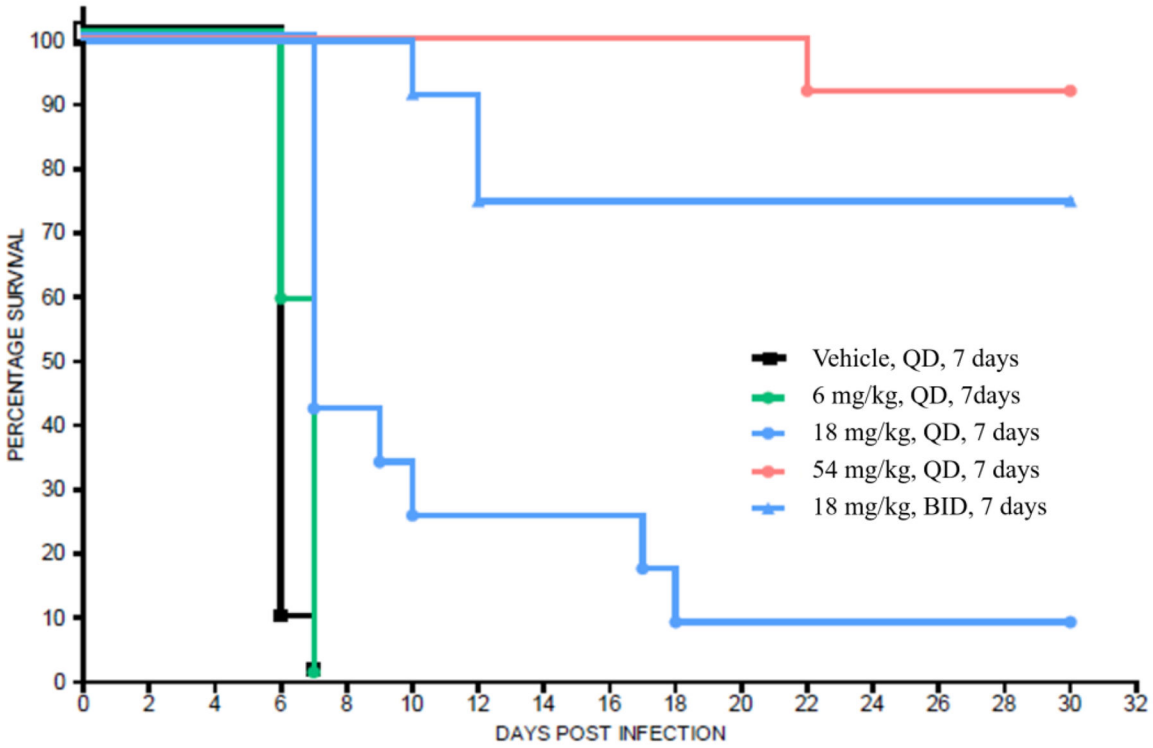

Figure 6a.

[a]Kaplan-Meier survival curves of compound **1** in CD-1 female mice (n = 12 for drug treated groups, n = 9 for vehicle group) infected with 3,000 RH type 1 *T. gondii* tachyzoites on day 0 followed by oral administration of **1** beginning on day 1 through day 7.

[a] Mice were carefully monitored for signs of infection, including by intermittently imaging (data not shown).

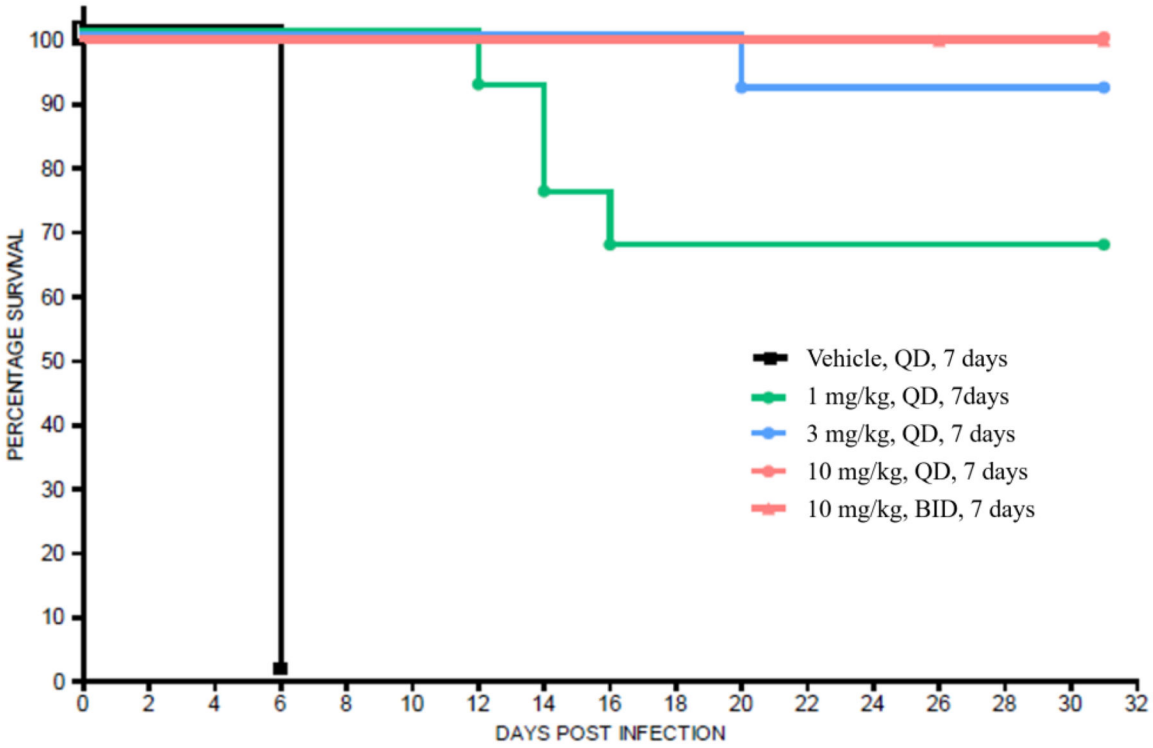

Figure 6b.

[a]Kaplan-Meier survival curves of compound **3** in CD-1 female mice (n = 12 for drug treated groups, n = 9 for vehicle group) infected with 3,000 RH type 1 *T. gondii* tachyzoites on day 0 followed by oral administration of **3** beginning on day 1 through day 7.

[a] Mice were carefully monitored for signs of infection, including by intermittently imaging (data not shown).

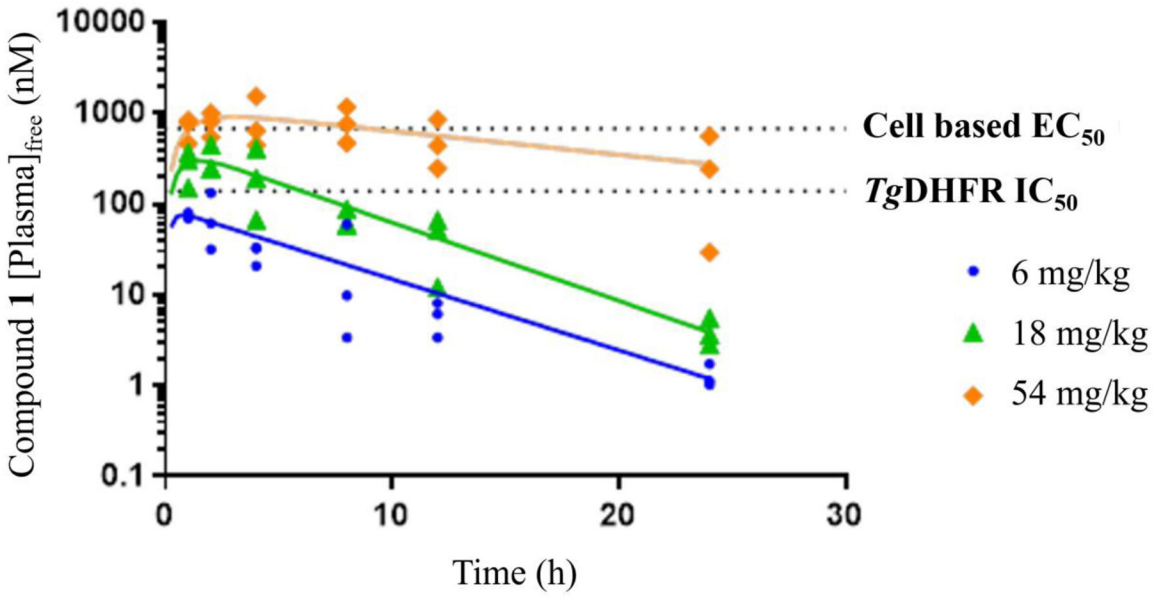

Figure 7a.

Day 4 $[plasma]_{free}$ exposure of **1** from the acute murine model of toxoplasmosis plotted as free plasma (nM) levels versus time.

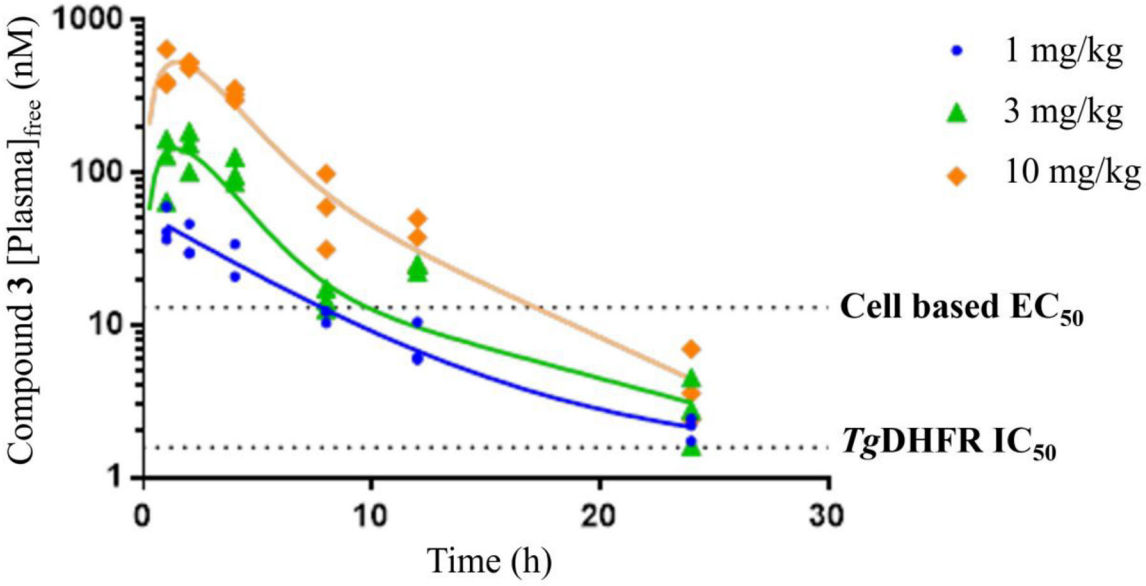

Figure 7b.

Day 4 $[plasma]_{free}$ exposure of **3** from the acute murine model of toxoplasmosis plotted as free plasma (nM) levels versus time.

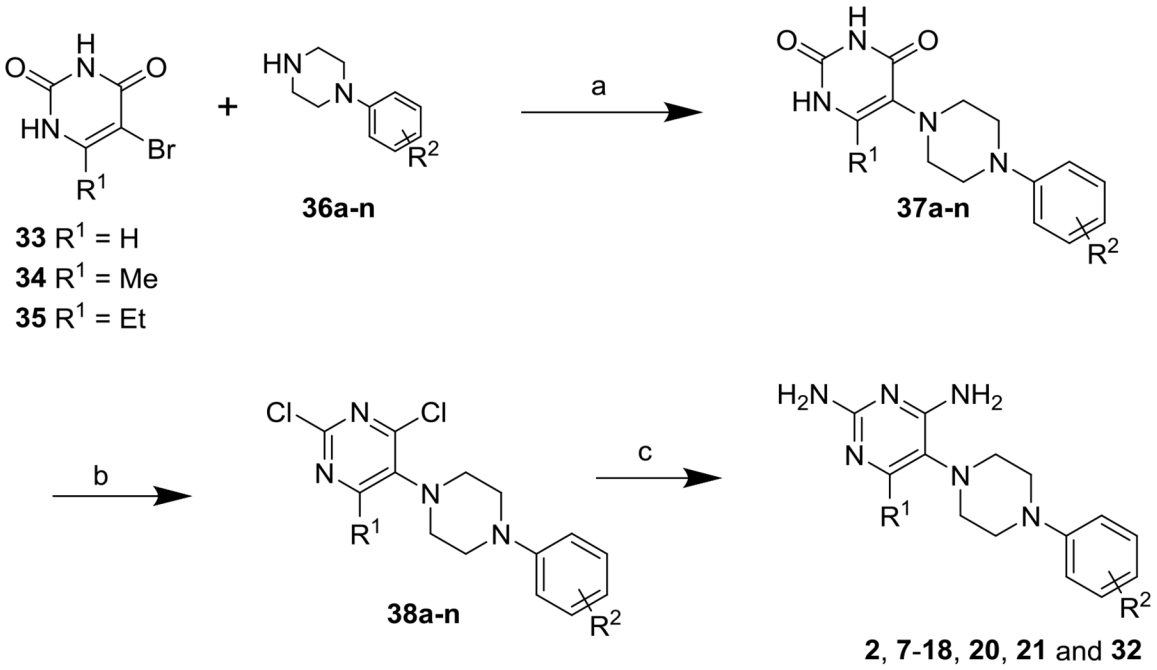

Scheme 1.

[a]Synthesis of Compounds **2**, **7**-**18**, **20**, **21** and **32**

R^2 = (a) 3-phenyl, (b) hydrogen, (c) 2-phenyl, (d) 4-phenyl, (e) 2-methyl, (f) 3-methyl, (g) 4-methyl, (h) 2-chloro, (i) 3-chloro, (j) 4-chloro, (k) 3-methoxy, (l) 3-trifluoromethyl, (m) 3-trifluoromethoxy, (n) 3-bromo

a Reagents and conditions: (a) KF, DMSO, 110 °C, 12 h; (b) $POCl_3$, DIPEA, 110 °C, 5 h; (c) NH_3, EtOH, 145 °C, 24 h

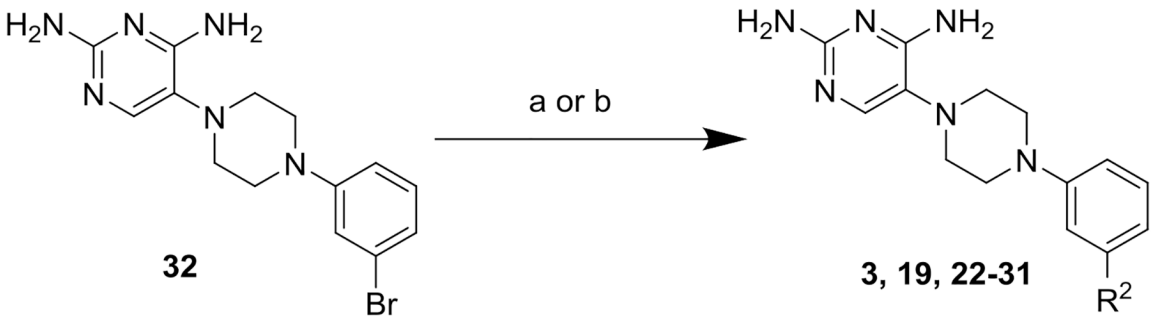

Scheme 2.

[a]Synthesis of Compounds **3, 19, 22–31**

R^2 = (o) 5-(2-methoxypyrimidine), (p) cyclopropyl, (q) 3-pyridine, (r) 4-pyridine, (s) 5-pyrimidine, (t) 4-pyridazine, (u) 5-(2-methylpyrimidine), (v) 5-(2-trifluoromethylpyrimidine), (w) 5-(2-cyclopropylpyrimidine), (x) 2-pyridine, (y) 2-pyrimidine and (z) 2-pyrazine.

a Reagents and conditions: (a) $Pd(PPh_3)_4$, R^2-$B(OH)_2$ (**39o-w**), Cs_2CO_3, Dioxane/H_2O, 110 °C; or (b) $Pd_2(dba)_3$, $Sn(nBu)_3$-R^2 (**40x-z**), Xphos, dioxane, 100 °C

Table 1.

Evaluation of Comparator Compounds on DHFR Inhibition, Kinetic Solubility, Clearance in Human Liver Microsomes and MDR1-MDCK Permeability

Compound	*Tg*DHFR[a] IC_{50} (nM)	*h*DHFR[a] IC_{50} (nM)	Selectivity Index[b]	Solubility[c] (μM)	HLM (mL/min/kg)	MDR1-MDCK[d]
1	139 ± 14	1680 ± 230	12	184	<8.6	36 (0.83)
2	8.76 ± 1.0	689 ± 39	79	3.9	28.4	2.7 (0.62)
4	33,100 ± 3400	503,000 ± 51,000	15	--	<8.6	7.5 (3.5)
5	78.3 ± 6.7	4.74 ± 0.36	0.061	--	--	--
6	1.35 ± 0.07	4.07 ± 0.11	3.0	--	--	--

[a] Average of at least 3 independent replicates ± SEM.

[b] Selectivity index (SI) is the *h*DHFR IC_{50}/*Tg*DHFR IC_{50}, determined within the same experiment.

[c] Kinetic solubility.

[d] A:B (papp 10^{-6} cm/sec) (ER), where ER is efflux ratio defined as permeability in A:B/B:A directions.

Table 2.

[a]Properties of **1** and **2**

Compound	MW	cLog P	Log P[b]	TPSA	cSol (μM)
1	248.7	3.00	2.71	76.8	135
2	346.4	3.74	3.38	83.2	3.09

[a]Calculated properties were performed using ChemDraw® Professional software version 17.0.0.206 (121).

[b]Measured LogP was performed at pH 11.0 in octanol/buffer.

Table 3.

Structure-Activity Relationships of phenylpiperazine analogs on inhibition of *Tg*DHFR and *h*DHFR

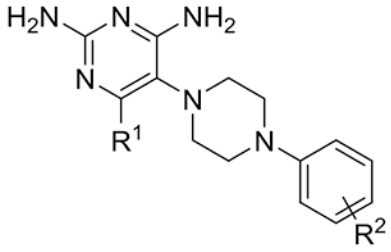

Compound	R^2	R^1	*Tg*DHFR[a] IC_{50} (nM)	*h*DHFR[a] IC_{50} (nM)	Selectivity Index[b]
2	3-phenyl	H	8.76 ± 1.0	689 ± 39	79
7	H	H	209 ± 28	12,500 ± 1200	59
8	2-phenyl	H	30.9 ± 2.2	1790 ± 190	58
9	4-phenyl	H	31.5 ± 2.7	347 ± 23	11
10	2-Me	H	>10,000	>30,000	Not available
11	3-Me	H	75.3 ± 5.5	5980 ± 320	79
12	4-Me	H	181 ± 14	3260 ± 110	18
13	2-Cl	H	>10,000	>30,000	Not available
14	3-Cl	H	39.8 ± 5.3	1540 ± 170	39
15	4-Cl	H	45.9 ± 7.3	1090 ± 140	24
16	3-MeO	H	57.8 ± 3.4	2710 ± 150	47
17	3-CF_3	H	62.1 ± 5.2	541 ± 43	8.7
18	3-CF_3O	H	12.9 ± 1.1	819 ± 36	63
19	3-cyPropyl	H	29.0 ± 1.7	1630 ± 45	56
20	3-phenyl	Me	9.19 ± 0.94	237 ± 21	26
21	3-phenyl	Et	3.91 ± 0.61	200 ± 16	51

[a] Average of at least 3 independent replicates ± SEM.

[b] Selectivity index (SI) is the hDHFR IC_{50}/*Tg*DHFR IC_{50}.

Table 4.

Evaluation of heteroaryl replacements of the distal phenyl of **2** on DHFR inhibition, selectivity, solubility, human liver microsomal clearance and MDCK-MDR1 permeability.

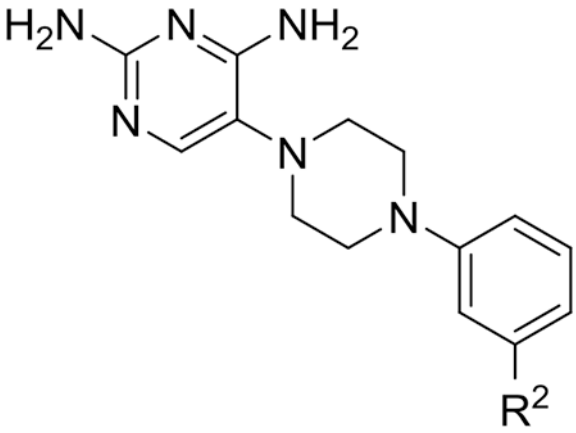

Compound	R^2	*Tg*DHFR[a] IC_{50} (nM)	*h*DHFR[a] IC_{50} (nM)	Selectivity[b]	Solubility[c] (μM)	HLM[d] (CLint)	MDR1-MDCK[e]
22	2-pyridine	10.3 ± 1.6	1360 ± 210	132	12	17.7	--
23	3-pyridine	2.68 ± 0.12	300 ± 55	112	--	--	--
24	4-pyridine	4.34 ± 0.43	468 ± 32	108	2.2	18.7	17.4 (0.86)
25	2-pyrimidine	27.3 ± 2.3	1300 ± 51	47.6	180	<8.6	31.7 (0.80)
26	5-pyrimidine	4.75 ± 0.34	1430 ± 100	301	>200	<8.6	20.2 (1.2)
27	2-pyrazine	10.3 ± 0.39	1330 ± 50	129	1.6	<8.6	19.3 (0.77)
28	4-pyridazine	6.00 ± 0.70	1100 ± 130	185	5.7	<8.6	6.40 (3.8)

[a] Average of at least 3 independent replicates ± SEM.

[b] Selectivity index (SI) is the *h*DHFR IC_{50}/*Tg*DHFR IC_{50}, determined within the same experiment.

[c] Kinetic solubility.

[d] HLM human liver microsomes, CLint intrinsic clearance (mL/min/kg),

[e] A:B permeability (papp 10^{-6} cm/sec), where ER is efflux ratio defined as permeability in A:B/B:A directions.

Table 5.

Evaluation of substitutions on the distal pyrimidine ring of **26** on DHFR inhibition, selectivity, solubility, human liver microsomal clearance and MDCK-MDR-1 permeability

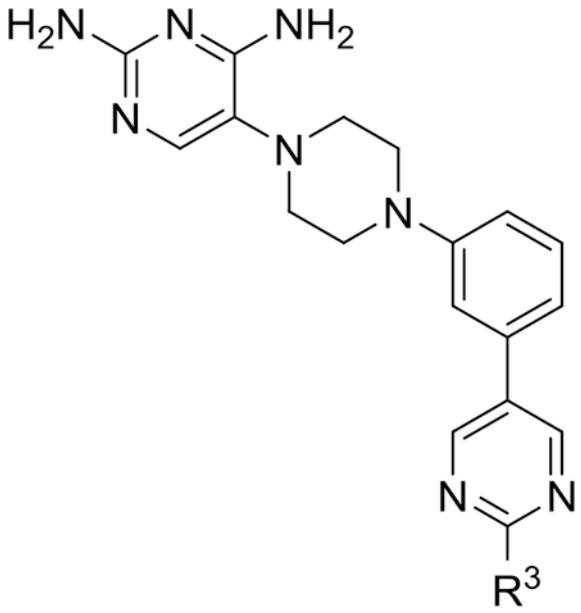

Compound	R^3	*Tg*DHFR[a] IC_{50} (nM)	*h*DHFR[a] IC_{50} (nM)	Selectivity index[b]	Solubility (μM)[c]	HLM[d] (CLint)	MDR1-MDCK[e]
29	Me	3.95 ± 0.26	935 ± 46	237	150	<8.6	19.3 (1.2)
3	MeO	1.57 ± 0.42	308 ± 71	196	186	<8.6	20.1 (1.1)
30	CF_3	32.7 ± 3.3	2800 ± 470	85.6	17	10.5	--
31	cypropyl	9.92 ± 0.83	973 ± 120	98	12	17.4	--

[a] Average of at least 3 independent replicates ± SEM.

[b] Selectivity index (SI) is the *h*DHFR IC_{50}/*Tg*DHFR IC_{50}, determined within the same experiment.

[c] Kinetic solubility.

[d] HLM human liver microsomes, CLint intrinsic clearance (mL/min/kg),

[e] A:B permeability (papp 10^{-6} cm/sec), where ER is efflux ratio defined as permeability in A:B/B:A directions.

Table 6

Parasiticidal activity for **1** and **3** in *T. gondii* infected human foreskin fibroblast cells as compared to the antiproliferative effects of **1** and **3** in MCF-7 cells

Compound	*T. gondii* Cell-Based EC_{50} (nM)[a]	MCF-7 EC_{50} (nM)[b]	Selectivity Index[c]
3	13 ± 3.8	7300	560
1	680 ± 210	11,700	17

[a] EC_{50}=half maximal response concentration, average of at least 3 experiments (± SD).

[b] MCF-7 cell viability determined using the MTT assay in triplicate (n = 1).

[c] Selectivity index calculated as the MCF-7 EC_{50}/*Tg* cell-based EC_{50}.

Table 7

[a]Growth effects of **3** on different strains of *T. gondii*

Strain	Host of origin	Geographic Distribution	Type	EC_{50} (nM)
GT1	goat	North America	1	18.0 ± 9.3
ME49	sheep	North America Europe	2	8.3 ± 2.9
RUB	human	South America	5	7.6 ± 3.3
VAND	human	South America	10	11.2 ± 0.5

[a]Average of at least 3 independent replicates ± SEM

Table 8

[a]Pharmacokinetics of compound **3** in mouse

Route	Dose (mg/kg)	%F	$C_{max, po}$ (ng/mL)	$T_{max, po}$ (h)	$AUC_{0\text{-}last, po}$ (ng•h/mL)	$CL_{, iv}$ (mL/min/kg)	$Vd_{, iv}$ (L/kg)	$t_{½, iv}$ (h)
IV	1.0	--	--	--	--	10.6	1.14	3.9
PO	0.83	47.3	178	0.05	750	--	--	--

[a]Oral bioavailability (%F), area under the concentration-time curve from time zero to the last measurable concentration ($AUC_{0\text{-}last}$), clearance (CL), maximum observed plasma concentration (C_{max}), intravenous (IV), per os (PO), elimination half-life ($t_{½}$), time to C_{max} (T_{max}), volume of distribution (Vd)